



January 2017

An Investigation Of The Impact Of Enso On Regional Climate Over The Northern Great Plains

Akila Sampath

Follow this and additional works at: <https://commons.und.edu/theses>

Recommended Citation

Sampath, Akila, "An Investigation Of The Impact Of Enso On Regional Climate Over The Northern Great Plains" (2017). *Theses and Dissertations*. 2143.

<https://commons.und.edu/theses/2143>

This Thesis is brought to you for free and open access by the Theses, Dissertations, and Senior Projects at UND Scholarly Commons. It has been accepted for inclusion in Theses and Dissertations by an authorized administrator of UND Scholarly Commons. For more information, please contact zeinebyousif@library.und.edu.

AN INVESTIGATION OF THE IMPACT OF ENSO ON REGIONAL CLIMATE
OVER THE NORTHERN GREAT PLAINS

by

Akila Sampath
Master of Science, Presidency College, 2007

A Thesis

Submitted to the Graduate Faculty
of the University of North Dakota

In partial fulfillment of the requirements

for the degree of

Master of Science

Grand Forks, North Dakota

May
2017

Copyright 2017 Akila Sampath

This thesis, submitted by Akila Sampath in partial fulfillment of the requirements for the Degree of Master of Science from the University of North Dakota, has been read by the Faculty Advisory Committee under whom the work has been done, and is hereby approved.



Dr. Jianglong Zhang (Chairperson)

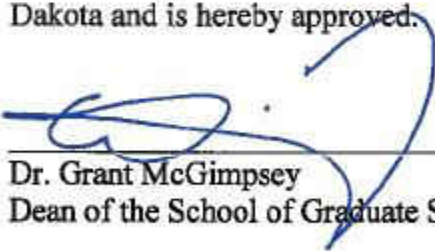


Dr. Gretchen Mullendore



Prof. Michael Poellot

This thesis is being submitted by the appointed advisory committee as having met all of the requirements of the School of Graduate Studies at the University of North Dakota and is hereby approved.



Dr. Grant McGimpsey
Dean of the School of Graduate Studies

January 19, 2017
Date

PERMISSION

Title: An Investigation of the Impact of ENSO on Regional Climate Over the Northern
Great Plains

Department: Atmospheric Sciences

Degree: Master of Science

In presenting this thesis in partial fulfillment of the requirements for a graduate degree from the University of North Dakota, I agree that the library of this University shall make it freely available for inspection. I further agree that permission for extensive copying for scholarly purposes may be granted by the professor who supervised my dissertation work or, in her absence, by the Chairperson of the department or the dean of the School of Graduate Studies. It is understood that any copying or publication or other use of this thesis or part thereof for financial gain shall not be allowed without my written permission. It is also understood that due recognition shall be given to me and to the University of North Dakota in any scholarly use which may be made of any material in my dissertation.

Akila Sampath
February 12, 2017

TABLE OF CONTENTS

LIST OF FIGURES	vii
LIST OF TABLES	x
ACKNOWLEDGEMENTS	xi
ABSTRACT.....	xii
CHAPTER	
I. INTRODUCTION	1
II. DATA AND METHODOLOGY.....	4
I. Surface Observations.....	4
II. Reanalysis Data	5
III. CMIP5 Models.....	5
a. CCSM4.....	6
b. CanCM4.....	7
c. EC-Earth.....	7
IV. Multivariate ENSO Index (MEI).....	8
V. Data Processing and Analysis Methods	9
a. Cressman Analysis of Ground Station Data.....	9
b. Ensemble Mean.....	10
c. Empirical Orthogonal Function (EOF)/Principle Component Analysis (PCA)	10
d. Presentation of EOF	11
e. Reconstruction Method	12
III. REGIONAL TEMPERATURE AND PRECIPITATION PATTERNS	15
3.1.1. Mean and Variance for the NGP's Temperature	15
3.1.2. Mean and Variance for the NGP's Precipitation	18
3.1.3. Trends in NGP's Temperature and Precipitation.....	21
3.1.4. Correlation between the NGP's Seasonal Climate and MEI	23

IV.	INVESTIGATION OF SEASONAL CLIMATE VARIABILITY ACROSS THE NGP THROUGH EOF ANALYSIS	25
	4.1.1. Prominent Patterns for the Temperature Field.....	26
	4.1.2. Prominent Patterns for the Precipitation Field.....	30
	4.1.3. Seasonal Trend Analyses and Potential Issues	35
	4.2. Time-series Analysis between the NGP's Climate Variability and MEI	38
	4.3. Potential Linkage of the NGP's Climate Variability (reconstructed) with the MEI Index.....	46
	4.3.1. Relationship between Temperature and MEI	47
	4.3.2. Relationship between Precipitation and MEI	51
V.	CONCLUSIONS.....	55
	REFERENCES	58

LIST OF FIGURES

Figure	Page
1. EOF patterns (a-c) of three modes for reanalysis DJF temperature (1965-2005) and their associated PCs (d-f). g) raw and h) reconstructed, temperature anomalies for 1965. i) regression and j) correlation maps, of the reconstructed DJF temperature anomalies and the MEI index (1965-05).....	13
2. Mean annual temperature (1965-2005) for the observations (a), reanalysis (b), and model simulations (c-e), as well as the standard deviation for the observations (f), reanalysis (g), and model simulations (h-j). Units are in °C.....	16
3. (Left, a-d) Temperature differences (°C) between observation and reanalysis as well as model simulations (1965-2005). (Right, e-h) Precipitation differences (mm) between observation and reanalysis as well as model simulations (1965-2005)	18
4. Mean annual precipitation (1965-2005) for the observations (a), reanalysis (b), and model simulations (c-e). The standard deviation for the observations (f), reanalysis (g), and model simulations (h-j) is also shown. Units are in mm	20
5. Long-term (left) trend (1965-2005) in temperature field for the observations (a), reanalysis (b), and model simulations (c-e). Units are in °C/41 years. Long-term (right) trend (1965-2005) in precipitation field for the observations (f), reanalysis (g), and model simulations (h-j) is also shown. Units are in mm/41 years.....	22
6. Spatial distribution of correlation between MEI and temperature (left) precipitation (right) for all four seasons.....	24
7. Regression of winter temperature anomalies onto associated three leading PCs: reanalysis (left) and model (right). The fractional variance explained by each mode is displayed in each panel's title. Units are in °C/standard deviation	28
8. Regression of spring temperature anomalies onto associated three leading PCs: reanalysis (left) and model (right). The fractional variance explained by each mode is displayed in each panel's title. Units are in °C/standard deviation	29
9. Regression of summer temperature anomalies onto associated three leading PCs: reanalysis (left) and model (right). The fractional variance explained by each mode is displayed in each panel's title. Units are in °C/standard deviation	29

10. Regression of autumn temperature anomalies onto associated three leading PCs: reanalysis (left) and model (right). The fractional variance explained by each mode is displayed in each panel's title. Units are in °C/standard deviation	30
11. Regression of winter precipitation anomalies onto associated three leading PCs: reanalysis (left) and model (right). The fractional variance explained by each mode is displayed in each panel's title. Units are in mm/standard deviation	33
12. Regression of spring precipitation anomalies onto associated three leading PCs: reanalysis (left) and model (right). The fractional variance explained by each mode is displayed in each panel's title. Units are in mm/standard deviation	33
13. Regression of summer precipitation anomalies onto associated three leading PCs: reanalysis (left) and model (right). The fractional variance explained by each mode is displayed in each panel's title. Units are in mm/standard deviation	34
14. Regression of autumn precipitation anomalies onto associated three leading PCs: reanalysis (left) and model (right). The fractional variance explained by each mode is displayed in each panel's title. Units are in mm/standard deviation	34
15. Normalized time series (1965-2005) of NGP's temperature (left column) and precipitation (right column). Units are in standard deviations	37
16. Normalized time series (1965-2005) of MEI and the NGP's temperature for Mode 1 (left column), Mode 2 (middle column), and Mode 3 (right column). The dark-shaded region corresponds to El-Niño events, and the light-shaded region corresponds to La-Niña events. Units are in standard deviations	44
17. Normalized time series (1965-2005) of MEI and NGP's precipitation for Mode 1 (left column), Mode 2 (middle column), and Mode 3 (right column). The dark-shaded region corresponds to El-Niño events, and the light-shaded region corresponds to La-Niña events. Units are in standard deviations	45
18. Regression patterns of four seasonal temperature anomalies with the MEI for 1965-2005: reanalysis (left) and model (right)	49
19. Correlation patterns of four seasonal temperature anomalies with the MEI for 1965-2005: reanalysis (left) and model (right)	50
20. Regression patterns of four seasonal precipitation anomalies with the MEI for 1965-2005: reanalysis (left) and model (right)	53

21. Correlation patterns of four seasonal precipitation anomalies with the MEI for 1965-2005: reanalysis (left) and model (right)	54
--	----

LIST OF TABLES

Table	Page
1. Percentage of the total variance explained by the first three seasonal EOFs	39
2. El-Niño and La-Niña events for the period of 1965-2005 (acquired From http://ggweather.com/enso/oni.htm)	39
3. Correlations between the first three EOF coefficient time series (1965-2005) and the MEI sequence of winter, spring, summer, and autumn when using the CMIP5 model, and reanalysis (a) surface temperature, (b) precipitation anomalies. Variances that correspond to each mode are displayed in parentheses beside the correlation coefficient. Correlation coefficients that exhibit a 95% significance level are highlighted in bold	40

ACKNOWLEDGEMENTS

This study was supported by NSF project IIA-1355466. I would like to thank my advisor, Dr. Jianglong Zhang, for his guidance and assisting me with this study. Throughout this work, Dr. Zhang has rendered his support in all possible ways to improve the content of the writing. I would also like to thank the other committee members, Dr. Gretchen Mullendore and Prof. Michael Poellot, for their suggestions and critiques that helped improve this manuscript. I would like to thank my friends and family for their love and for supporting me every step of the way.

ABSTRACT

Using ground-based observations, as well as reanalysis and Coupled Model Intercomparison Project Phase 5 (CMIP5) data, the long-term changes in precipitation and surface temperature are studied for the Northern Great Plains (NGP) region for the period of 1965-2005. Significant positive trends of $\sim 1-2$ °C/41 years in annual mean temperature are found across North Dakota and Minnesota. This study also suggests that the eastern part of the NGP region is wetter than the western part of the NGP, for the past 41 years. In addition, the spatial-temporal changes of precipitation and temperature of the region, as well as their linkages to Multivariate El-Niño-Southern Oscillation (ENSO) Index (MEI), are investigated through empirical orthogonal function (EOF) analysis using reanalysis and CMIP5 data. The NGP's temperature field exhibits larger increasing trends in the winter season, while the largest variations in precipitation are found for the summer season. This study further indicates that MEI is positively correlated with winter temperature in North Dakota, and ENSO could also be associated with variations in summer precipitation of the NGP region.

CHAPTER I

INTRODUCTION

The objective of this study is to analyze variations in climate across the Northern Great Plains (NGP) region and then investigate the linkage between the regional climate of NGP and large scale dynamics, using Coupled Model Intercomparison Project Phase 5 (CMIP5) model simulations, reanalysis, and observational data for a forty one-year period (1965-2005). The NGP region includes North Dakota, South Dakota, Montana, Nebraska, and Minnesota, and is one of the largest agricultural producers in the United States. The NGP agricultural sector has a considerable impact on the NGP's economy with a significant contribution from North Dakota's agriculture industry (Gary Vocke and Mir Ali 2013). Climate variability is one of the critical factors that determine the agricultural production across the NGP, and consequently, the economy of NGP's agricultural sector. For example, the estimated monetary loss due to crop destruction by severe drought was \$223 million for 2002 and \$425 million for 2006 (North Dakota Department of Agriculture 2007). Also, the observed excess summer rainfall across North Dakota has damaged the spring wheat harvest (G. C. Bora et al. 2014). Thus, it is necessary to study variations in temperature and precipitation fields on both spatial and temporal scales across the NGP.

Many past studies have demonstrated the large dependency of crop production for a given growing season on temperature and precipitation (e.g., Lobell and Asner 2003; Lobell et al. 2007; Keller and Niyogi 2014). Specifically, Lobell and Asner (2003) found an approximately 17% relative decline in both corn and soybean yields in the U.S. for

each degree rise in growing season temperature. In addition, Lobell et al. (2007) examined 12 leading Californian crops and found that precipitation accounted for more than 60% of the variance in most of the crop yields. Thus, as one of the focuses of this study, means, variances, and trends of precipitation and temperature are studied for the NGP region with the use of both observational and modeling datasets.

Another focus of this work is to examine the association of regional precipitation and temperature variations with El Niño-Southern Oscillation (ENSO), which is very often considered a key driving force of regional climate variability across the globe (Goddard et al. 2001). For example, Namias (1982) found coherent positive and negative correlation patterns between the summer temperature field of the Great Plains and the North Pacific sea surface temperature (SST). Ropelewski and Halpert (1986) explained the teleconnection between both North American precipitation and temperature patterns and ENSO anomalies. They found that above normal precipitation is associated with April through October of ENSO year (1931-1984), and also October of the ENSO year to March of the non-ENSO year (from 1875-1980). Yet another study, Bunkers et al. (1996), demonstrated the association of ENSO (warm phase) and the La Niña Southern Oscillation (LNSO; cold phase) with Northern Plains precipitation and temperature observations for the period of 1880-1990. They found a significant increase in precipitation for April through October during ENSO, but a significant decrease in precipitation for May through August during LNSO. Their study also suggested a tendency of warmer winters across the Northern Plains; however, this finding is not statistically significant.

Thus, using both observational-based and modeling-based data for the past 41 years, this study focuses on investigating two research questions in relating climate variations of the NGP region:

(1) What are the variations in temperature and precipitation for the past 41 years over the NGP region? Can agreement be achieved among analyses from model-, reanalysis- and observational-based data?

(2) What are the linkages between ENSO and the temporal-spatial variations of precipitation and surface temperature across the NGP region?

To assist the analysis, statistical parameters such as the climate mean and standard deviation, and statistical methods like the Empirical Orthogonal Function (EOF) and correlation techniques, are used to identify variations in the NGP's climate. Furthermore, reconstruction of all fields has been completed to explain the linear relationship between ENSO and regional climate variability.

This thesis is structured as follows: Chapter 2 provides an explanation of the datasets and methods used. Chapter 3 studies the spatial and temporal variabilities in precipitation and temperature fields over the NGP region. Chapter 4 examines the seasonal-based regional climate variability through an EOF analysis. The covariability between the Northern Plain's seasonal precipitation, surface temperature patterns, and Multivariate ENSO Index (MEI) anomalies are also studied. The linear relationship between MEI and the Northern Plain's reconstructed surface temperature and precipitation patterns is further explored. A summary with some discussion is also presented in Chapter 5.

CHAPTER II

DATA AND METHODOLOGY

This study uses both observational and model data for the analysis of climate variations across the NGP region for the period of 1965-2005. The temperature and precipitation data are obtained from land-based stations across the NGP, National Centers for Environmental Prediction (NCEP), and National Center for Atmospheric Research (NCAR) reanalysis, and CMIP5 model simulations. The three different Global Climate Model (GCM) simulations used in this study are the Community Climate System Model Version 4 (CCSM4), the Fourth Generation Canadian Coupled Global Climate Model (CanCM4), and the European Earth System Model (EC-Earth). In addition, the MEI index is used to study the association of ENSO to the climate of the NGP region.

I. Surface Observations

Daily precipitation, and minimum and maximum temperature data were obtained from the National Oceanic and Atmospheric Administration (NOAA) National Climate Data Center (NCDC 2000a). Measurements from 391 ground stations across the NGP were selected from the Historical Climatology Network. Ground-based observations are often considered as “ground-truth” in the evaluation of model simulations. However, limitations of ground-based temperature and precipitation data include gaps in less populated regions (especially in the Northern Hemisphere) and erroneous observations due to problematic equipment.

II. Reanalysis Data

NCEP/NCAR (Kistler et al. 1999) surface temperature and precipitation reanalysis data are obtained on a T62 Gaussian grid over the Northern Plains. The NCEP/NCAR reanalysis (R1) model with T62 Gaussian grids and 28 vertical sigma levels represents the state of the Earth's atmosphere, incorporating land surface, ship, rawinsonde, pibal (Pilot Balloon Data), aircraft, and satellite observations from 1948-present into a frozen state-of-the-art global data assimilation system.

III. CMIP5 Models

The Coupled Model Intercomparison Project Phase 5 (CMIP5) project (Taylor et al. 2012), integrates about 50 climate modeling groups around the world to address major scientific questions that were prompted during the Intergovernmental Panel on Climate Change Fourth Assessment Report (IPCC AR4) evaluation process, to better understand climate, and to provide an improved projection of future climate change.

Three CMIP5 model simulations, CCSM4, CanCM4, and EC-Earth, were randomly selected based on the study results of North American Climate in CMIP5 Experiments (Sheffield et al. 2013a) to take advantage of different climate modelling strategies developed across the nations. Some considerations went into “randomly” selecting the models initialized from the historical simulations (Taylor et al. 2009). For example, these historical period simulations are performed with atmospheric-ocean global climate models (AOGCMs). These simulations are forced by estimations of historical changes in atmospheric composition from natural and anthropogenic sources, volcanoes, greenhouse gases, and aerosols, as well as changes in solar output and land

cover. Historical simulations were obtained for the period of 1965-2005, and are also initiated using the r3i1p1 (third realization of the first version of the perturbed physics model) ensemble member. Note that to study the impact of ENSO on regional climate, it is recommended to use Atmospheric Model Intercomparison Project (AMIP) data, which are climate model simulations with the use of observed sea surface temperature forcings. However, AMIP data are not used in this study, as the data record is not long enough to cover the period of this study (Taylor et al. 2009). In addition, CMIP5 data are considered as a secondary dataset in this study, and are used for a comparison (e.g., comparing with reanalysis data-based estimates) purpose only.

These data were downloaded from the Earth System Grid - Center for Enabling Technologies (ESG-CET), on the page <http://pcmdi9.llnl.gov/>. The initial interest was to acquire knowledge of the quality of cloud area fraction, air temperature, near-surface temperature, surface temperature, convective precipitation, and precipitation from different models, however this was later restricted to only precipitation and surface temperature from CCSM4, CanCM4, and EC-Earth models.

a. CCSM4

The Community Climate System Model Version 4 (CCSM4) is a fully coupled model consisting of the atmosphere, land, ocean, and sea ice components. It has 26 vertical levels with a finite volume dynamical core coupled to the x1 ocean and ice models (FV2x1). This model includes a newly updated deep convective parameterization scheme which improves the representation of the ENSO events in model simulations in comparison with CCSM3 (Gent et al. 2011). The indirect effects of aerosols, however,

are not included, which may introduce a high bias in the simulated surface temperature (Gent et al. 2011). The spatial resolution of CCSM4 model data is 0.94° by 1.25° latitude/longitude grid. CCSM4 includes improvised El Niño/Southern Oscillation (ENSO) representation and ocean mixing (Shields et al. 2012).

b. CanCM4

The Fourth Generation Canadian Coupled Global Climate Model (CanCM4) (Lohmann and Roeckner 1996) has 35 vertical levels. In this model, the atmospheric component of CanAM4 is coupled with an oceanic component of CanOM4 (Merryfield et al. 2013). The spatial resolution of CanCM4 model data is 2.8° latitude/longitude grid for both precipitation and surface temperature. It is also modernized by including the physical parameterization schemes of the correlated-k distribution to represent the mixing between the surface mixed layer and ocean interior (Merryfield et al. 2013) and single-moment cloud microphysics scheme (Lohmann and Roeckner 1996; Rotstayn 1997; Khairoutdinov and Kogan 2000), as well as an updated shallow convection scheme (von Salzen et al. 2005).

c. EC-Earth

The European Earth System Model (EC-Earth) includes the atmospheric component as the European Centre for Medium Range Weather Forecasts (ECMWF) (Hazeleger et al. 2010) with Integrated Forecast System (IFS) model version 31r1 and ocean component as the Nucleus for European Modelling of the Ocean (NEMO). The spatial resolution of EC-Earth is 1.125° latitude/longitude grid (T159/N80 Gaussian

grid), and this model features 62 vertical levels. NEMO has 1° spatial resolution with 42 vertical levels. The OASIS 3 coupler is used to couple the ocean/ice model with the atmosphere/land model. EC-Earth model also includes the enhanced version of convection and land surface parameterization scheme. This model approximates the 3D Navier-Stokes equations, and dynamics of the atmospheric components are computed using a spectral method. EC-Earth is based purely on the concept of seamless prediction that establishes forecasting of weather and study of climate change into a single framework.

IV. Multivariate ENSO Index (MEI)

The MEI index is used here to represent the tropical Pacific variables of atmospheric and oceanic components. The MEI is considered to be the most representative of many conventional ENSO indices (COADS; Wolter and Timlin 1998). The MEI is acquired from <http://www.esrl.noaa.gov/psd/enso/mei/table.html> for the period of 1965-2005. This index favors the specialized application of examining the covariability between ENSO and a specific region of the globe. The advantage of using MEI for this study is to consider both temporal and magnitude factors of El Niño and La Niña events. MEI is a derived product from the tropical Pacific Comprehensive Ocean-Atmosphere Data Set (COADS; Wolter and Timlin 1998). The expansion coefficients of MEI are constructed with six distinct features of climate variability over the Tropics. MEI includes the first principal component of sea-level pressure (P), zonal (U) and meridional (V) wind components, sea surface temperature (S), surface air temperature (A), and total cloudiness fraction of the sky.

V. Data Processing and Analysis Methods

a. Cressman Analysis of Ground Station Data

Ground-based precipitation and temperature data are obtained from 391 ground stations across the NGP region. Prior to applying the data in this analysis, the dataset has gone through quality assurance steps. Specifically, these data were checked for inconsistencies, such as consecutive days with the same value for each variable, or for when the maximum temperature is less than the minimum temperature. If any suspect stations with consecutive days of zero rainfall values exist, those values are ignored.

Firstly, daily temperature values of observation data are computed by averaging the daily minimum near-surface air temperature and daily maximum near-surface air temperature. Secondly, the monthly mean temperature of observation data is computed by averaging the daily temperature values of that specific month. While in precipitation field, monthly values of observations are computed by summing the daily precipitation values of that specific month. To inter-compare observations with CMIP5 monthly model simulations and reanalysis monthly data, the Cressman (Cressman 1959) interpolation scheme is applied to resample ground-based observations into 0.025° latitude/longitude gridded data. Still, it is worth noting that the observational-based monthly means may not match monthly means from reanalysis and CMIP5 data (e.g., average results from all time steps) due to possible different methods in constructing monthly means. This may introduce a sampling related bias in this study.

In Cressman analysis, Cressman weights ($w(r)$) determined based on the distance r between the analysis location \mathbf{r} and the observation location \mathbf{r}_j :

$$r = | \mathbf{r} - \mathbf{r}_j | \quad (1)$$

$$w(r) = \frac{R^2 - r^2}{R^2 + r^2}, \text{ for } r < R \quad (2)$$

$$= 0, \text{ for } r \geq R \quad (3)$$

where r is the distance between an observational point and a given grid point, and the radius of influence R is set to 2° latitude/longitude. In order to ensure there is no bias, weights have to be scaled by their sum:

$$W_j = \frac{w_j}{\sum_j w_j} \quad (4)$$

b. Ensemble Mean

The ensemble mean is computed using CCSM4, CanCM4, and EC-Earth data. Since the spatial resolution of these three models is different from each other, it is necessary to re-grid them to a consistent spatial resolution 2.8° latitude/longitude grid (a 128×64 grid) using a bilinear method. The ensemble mean is obtained by averaging the three model simulations with a consistent spatial resolution.

c. Empirical Orthogonal Function (EOF)/Principle Component Analysis (PCA)

In this study, Empirical Orthogonal Function (EOF)/Principle Component Analysis (PCA) (Dommenges, A. and M. Latif 2002) is used to study the climate variability of NGP with the CMIP5 ensemble mean as well as reanalysis data. Prior to

EOF analysis, seasonal means are computed using both datasets for DJF (December, January, February), MAM (March, April, May), JJA (June, July, August), and SON (September, October, November). These data are then deseasonalized by subtracting the long-term mean from each month. When studying the association of CMIP5 data with ENSO, the data are further de-trended. Before applying EOF analysis on any portion of the globe, the observations are also weighted using the square root of the cosine of the latitude. This area weight is to account for the change in grid size in the convergence zone of the meridians. Following the computation of the covariance matrix of the data matrix, the eigenvector and eigenvalues are then computed to determine the variances in spatial patterns. Then the eigenvector associated with each eigenvalue is normalized to unit length to obtain EOF spatial patterns. The fraction of the total variance explained by each mode is equal to the ratio of each eigenvalue to the sum of all eigenvalues. Additionally, to understand the variation of EOF (x, y) spatial patterns over time, principal component (PC (t)) is computed by projecting eigenvectors (EOF) onto the anomaly field of the original data. In this study, three leading EOFs are computed.

d. Presentation of EOF

The principle components (PCs) are then normalized (i.e., standardized anomalies) by dividing them by their respective standard deviations. These temporal anomalies are then multiplied with their respective area averages to represent them as a time series. An advantage of representing PCs in units of standardized anomalies is that events with higher or lower amplitudes are easily distinguishable. Also, in this study, the spatial patterns of EOFs are represented by homogeneous regression maps. The homogeneous regression

maps are constructed by projecting standardized PCs onto the original data anomalies. The homogeneous regression maps show EOF spatial patterns with physically meaningful units associated with the input data per standard deviation. Also, one standard deviation represents a typical fluctuation in the base index time series.

Also, the correlation coefficients between the principle component of each mode of each field and the MEI index are computed. The statistical significance of the correlation coefficients is determined by a student's t-test, as described by Haan (2002). The degree of degeneracy of EOF analysis is assessed using the "rule of thumb" suggested by North et al. (1982). The North test is used to compute 95% significance errors of the estimated eigenvalues and to detect eigenvectors that are not distinct (with overlapping error bars).

e. Reconstruction Method

One major application of EOF analysis is to create a new field by reconstruction. A new data field is created by projecting the first three leading EOF spatial patterns onto an associated amplitude of the time series. All the fields are quantified through EOF reconstruction:

$$X'(x, y, t) = \sum_{m=1}^N EOF_m(x, y) \cdot PC_m(t) \quad (5)$$

where m is the number of eigenvalues, $X'(x, y, t)$ is the reconstructed field as a function of time (t) and space (x, y). Here, the EOF spatial pattern is projected upon the associated principle components to produce a new field. These reconstructed data are a function of both time and space with an enhanced mode of higher variability.

Using the DJF temperature as an example, Fig. 1 shows the steps of creation of the reconstructed fields. Figures 1a-c show the first three modes of EOF spatial patterns, and Figs. 1d-f show the associated principle components using the reanalysis data for the study period of 1965-2005. The raw and reconstructed temperature anomalies for the year of 1965, based on Equation 5, are shown in Figures. 1g and 1h.

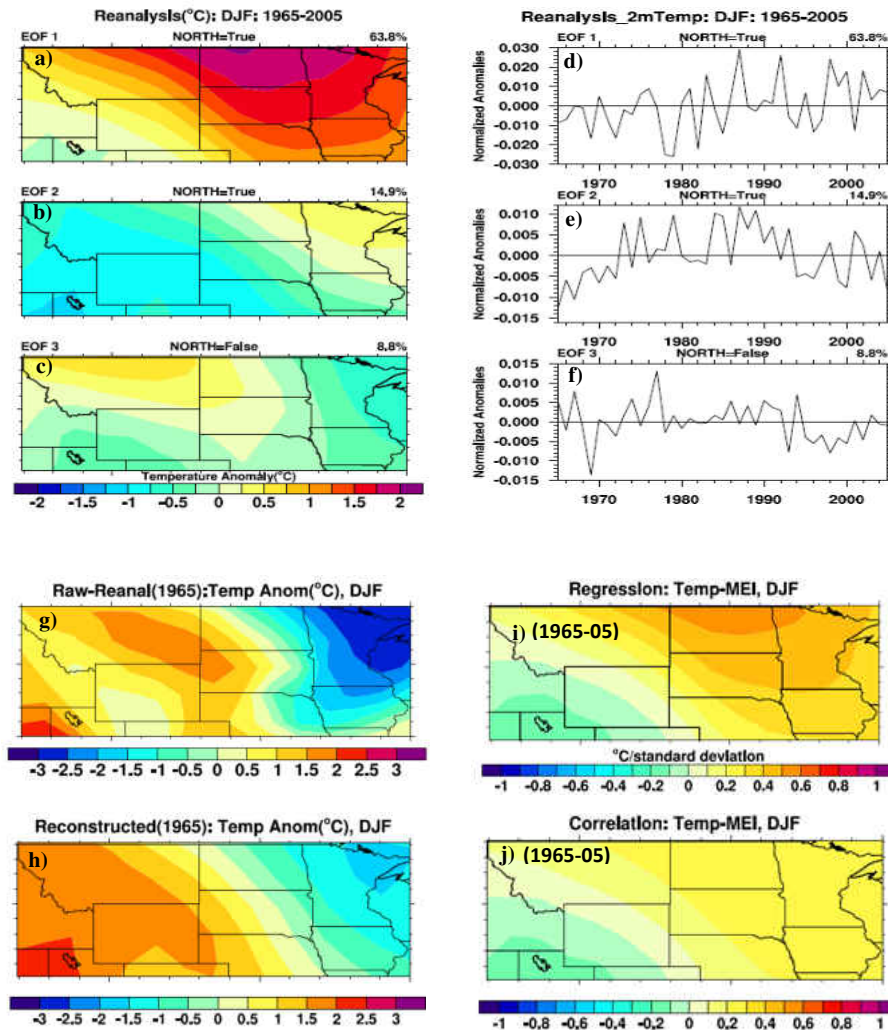


Figure 1. EOF patterns (a-c) of three modes for reanalysis DJF temperature (1965-2005) and their associated PCs (d-f). g) raw and h) reconstructed, temperature anomalies for 1965. i) regression and j) correlation maps, of the reconstructed DJF temperature anomalies and the MEI index (1965-05).

To gain insight of the reconstructed anomaly fields in representing large scale ENSO variability, the heterogeneous correlation and regression maps are constructed between the reconstructed field and the expansion coefficients of MEI. If the correlation or regression is computed between two different variables, then that is named as heterogeneous correlation or regression map.

$$u_k = \frac{1}{N\sigma_k} X y_k^{*T} \quad (6)$$

where N is sample dimension, u_k is the regression or correlation values for the k time period and σ_k is the standard deviation of time series, X is the reconstructed field, and y_k^{*T} is the expansion coefficient of MEI.

The regression map helps to obtain reconstructed anomalies that are associated with the variation in the expansion coefficient of MEI (Dommenget, D. and M. Latif 2002), while the correlation map reveals the significance of the regression map (Trenberth et al. 2002). Again, for illustration purposes, Figs. 1i and 1j show the regression and correlation maps respectively, based on Equation 6, using MEI and the reconstructed DJF temperature anomalies.

CHAPTER III

REGIONAL TEMPERATURE AND PRECIPITATION PATTERNS

In this section, the long term means and variations of the temperature and precipitation fields are studied over the NGP using ground-based, reanalysis, and CMIP5 data. Trends in temperature and precipitation for the past 41 years are evaluated and results from three different datasets are also inter-compared. Lastly, a linear regression method is applied to study the correlation between MEI and regional climate of the NGP. Note that some similar steps are also performed in the next chapter, but with the use of the EOF analysis. Results from this section can be considered as a cross-check for the EOF-based analysis as mentioned in the next chapter.

3.1.1. Mean and Variance for NGP Temperature

The long-term temperature means for observations, reanalysis, and model simulations are shown in Fig. 2 (a-e). The annual mean temperature patterns from reanalysis and GCM model data are similar. The temperature field displays a latitudinal pattern and the southern part of the NGP is warmer than its northern counterpart. Moreover, both observation (Fig. 2a) and reanalysis data (Fig. 2b) report the maximum mean temperature of ~ 10 °C over the southeast part of the NGP (e.g., Nebraska), while CCSM4 (Fig. 2c) and CanCM4 (Fig. 2e) models overestimate the maximum mean temperature by ~ 5 °C. Still, the 5 °C difference may partially be caused by the difference in constructing monthly means as mentioned before. For illustration purposes, Fig. 3 (left) shows the differences in mean annual temperature between the observations and

reanalysis as well as GCM model simulations. Not surprisingly, larger negative differences are found between observations

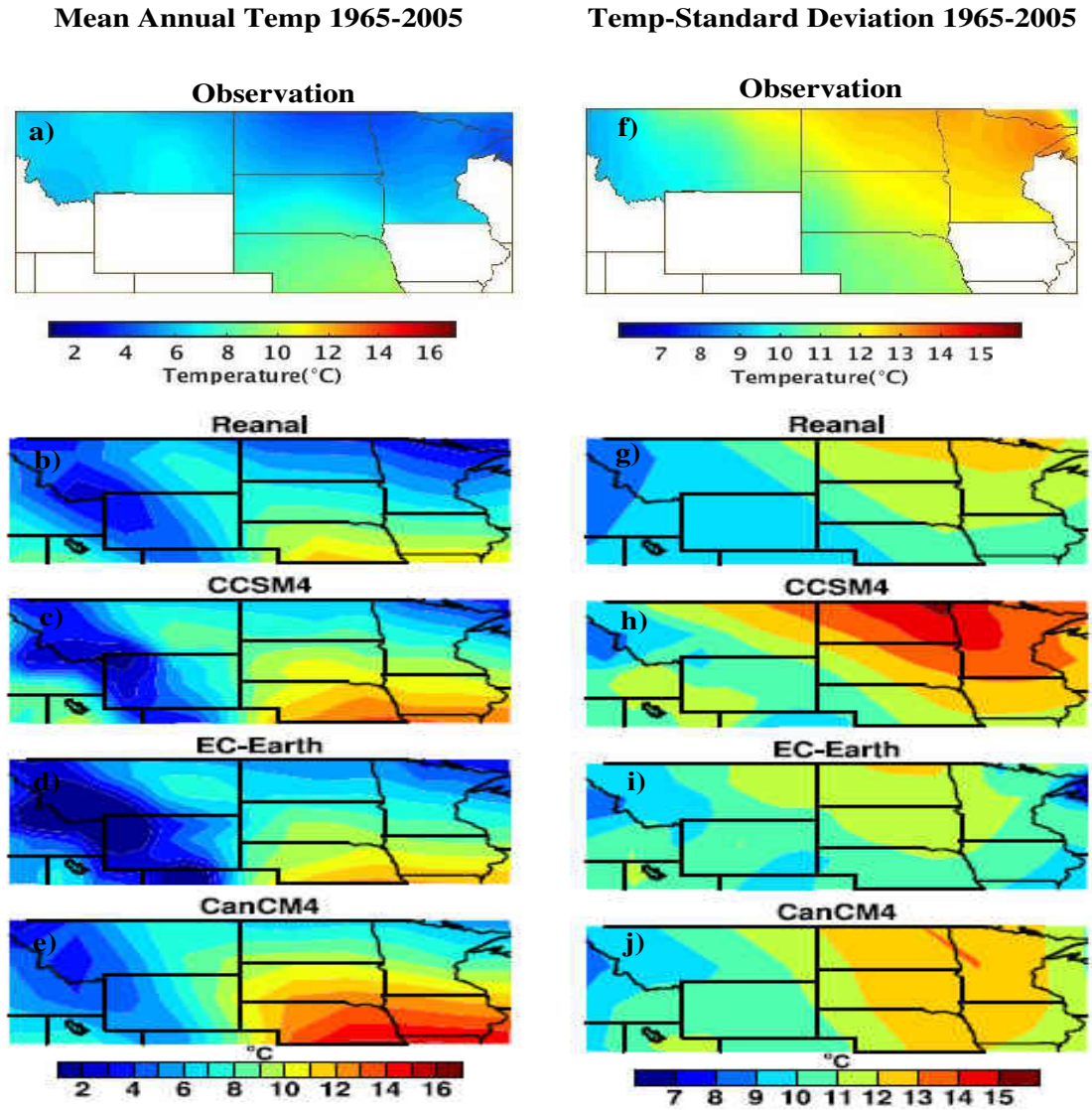


Figure 2. Mean annual temperature (1965-2005) for the observations (a), reanalysis (b), and model simulations (c-e), as well as the standard deviation for the observations (f), reanalysis (g), and model simulations (h-j). Units are in °C.

and GCM model simulations (Figs. 4b-4d), over the southern part of the NGP region. Figure 2 (f-j) shows the standard deviation for the temperature field. Consistently, a larger variability of 11 °C to 14 °C is found over North Dakota and Minnesota for all datasets. The regions with the maximum temperature variability, however, do not coincide with regions that exhibit the maximum annual mean temperatures. Specifically, over North Dakota, a moderate mean temperature, which ranges from 4 to 6 °C, is found from observational and reanalysis data. The maximum standard deviation for the same region, however, is found to range from 11 to 13 °C.

Mean temperature difference 1965-2005

Mean Precipitation difference 1965-2005

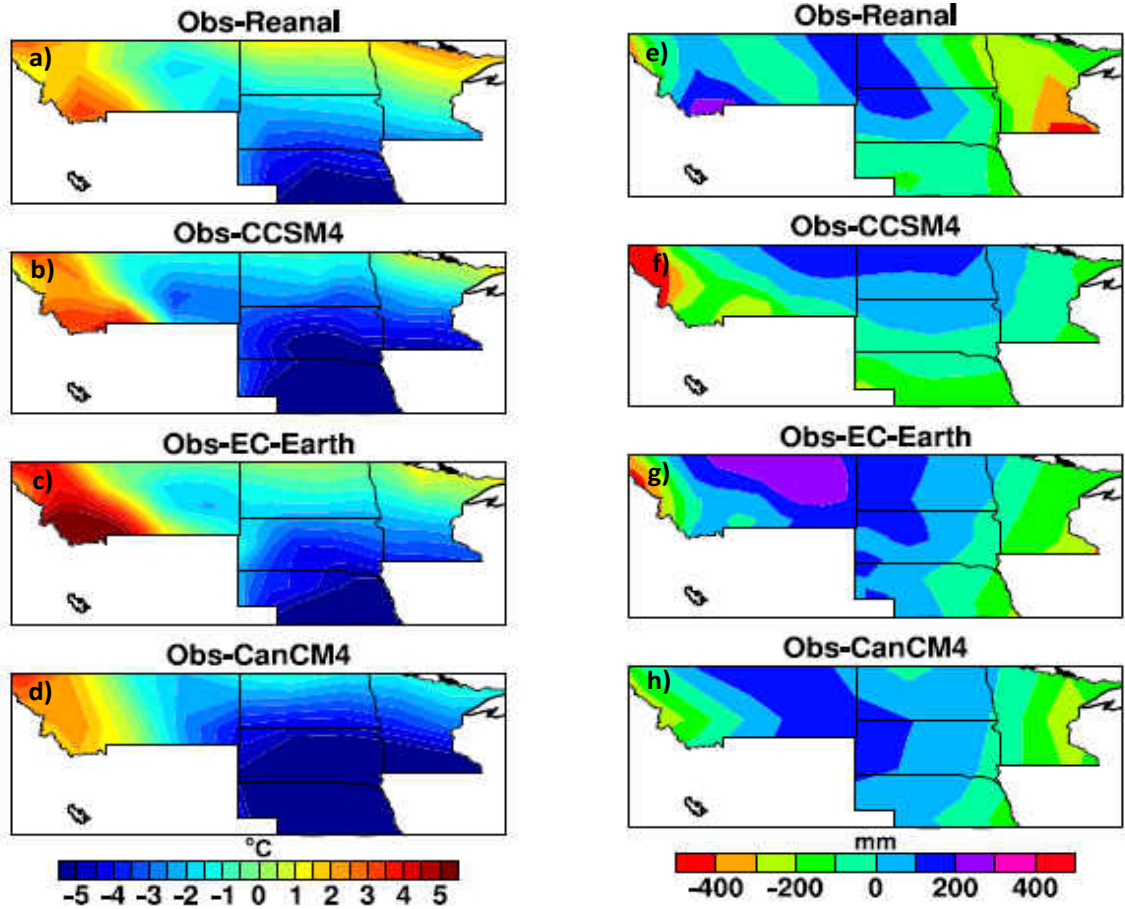


Figure 3. (Left, a-d) Temperature differences ($^{\circ}\text{C}$) between observation and reanalysis as well as model simulations (1965-2005). (Right, e-h) Precipitation differences (mm) between observation and reanalysis as well as model simulations (1965-2005).

3.1.2. Mean and Variance for the NGP's Precipitation

The mean annual cumulative precipitation patterns estimated from observations, reanalysis, and model simulations for the study period of 1965-2005 are shown in Fig. 4 (a-e). All datasets suggest that the eastern part of the NGP received 40-60% more annual mean cumulative precipitation than the center and western part of the NGP region. Also, consistent patterns are observed between the reanalysis (Fig. 4b) and model simulations

(Figs. 4c-4e). Furthermore, the maximum mean cumulative precipitation of 400 mm to 650 mm is found over the central portion of the NGP for all datasets. Again, the differences in mean annual cumulative precipitation between the observations and reanalysis as well as model simulations are shown in Fig. 3 for illustration purposes. Figure 4 (f-j) shows the standard deviation for the precipitation field. In contrast to the temperature field, regions with the maximum mean cumulative precipitation are also regions with the maximum precipitation variability. Specifically, a moderate mean cumulative precipitation of 400 mm - 500 mm, with a moderate standard deviation of 100 mm - 150 mm, is found over North Dakota from all datasets.

Mean Annual Precip 1965-2005

Precip-Standard Deviation 1965-2005

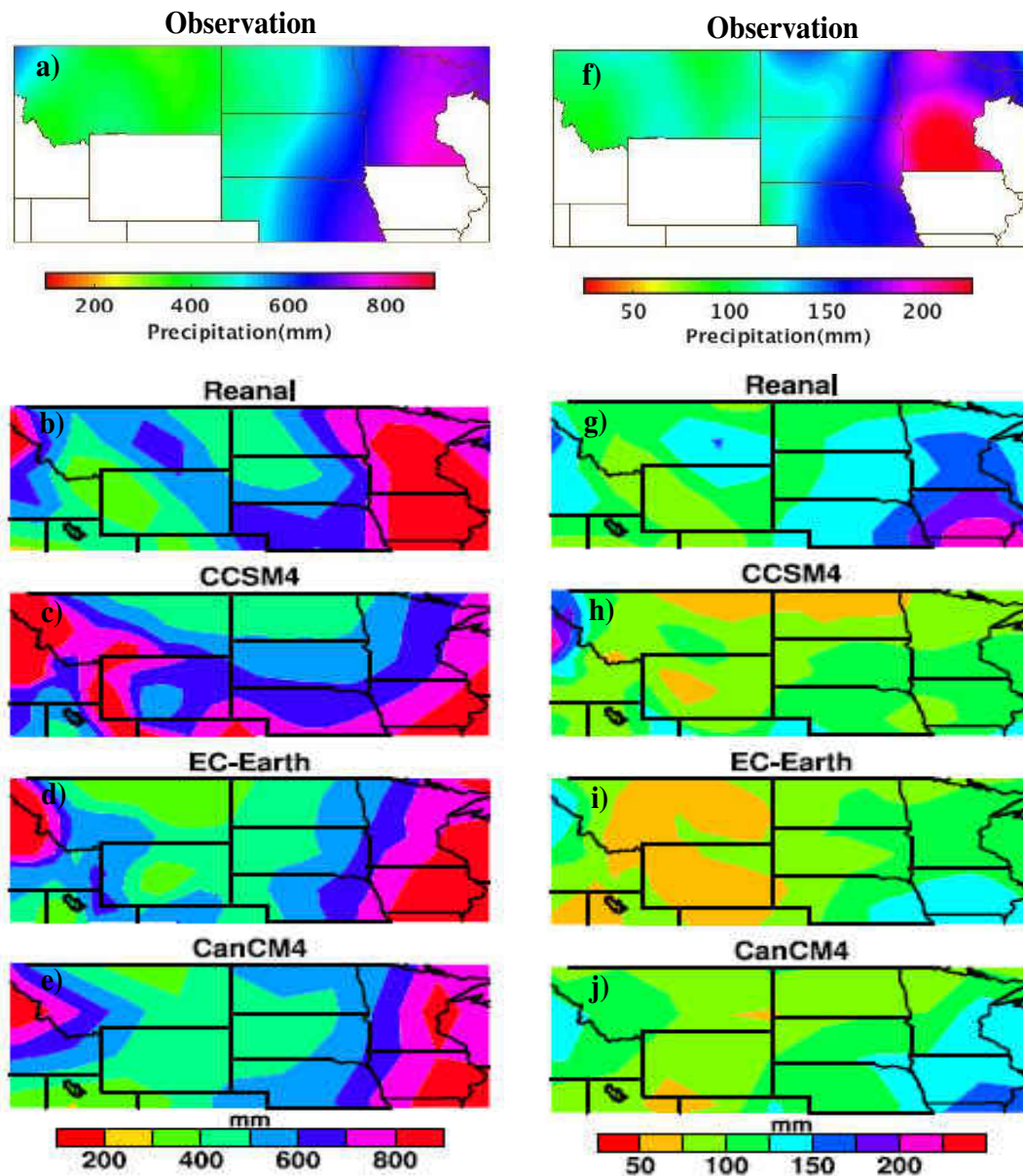


Figure 4. Mean annual precipitation (1965-2005) for the observations (a), reanalysis (b), and model simulations (c-e). The standard deviation for the observations (f), reanalysis (g), and model simulations (h-j) is also shown. Units are in mm.

3.1.3 Trends in NGP's Temperature and Precipitation

In addition to the analysis of mean temperature and precipitation patterns and their inter-annual variability as mentioned from the previous section, the long-term trends of mean annual cumulative precipitation (Fig. 5, left) and mean annual temperature (Fig. 5, right) for the NGP region are detailed in this section. A positive trend of 1-2 °C/41 years is observed in mean annual temperature across western Montana, North Dakota, and Minnesota from all data (Figs. 5a -5e). Results from this study are in good agreement with previous findings (e.g., Folland et al. 2001). While the temperature trends are largely consistent across the NGP region, distinct trends in annual mean cumulative precipitation are found for the eastern versus the western part of the NGP. Positive precipitation trends of 50 mm - 200 mm/41 years are found over the eastern part of NGP, yet negative precipitation trends of around -100 mm/41 years are shown for the western part of NGP using observational-based data (Fig. 5f). This analysis suggests a wetter eastern part and a drier western part of the NGP for the past 41 years. Also, the long-term trends estimated from observations are rather different from model-based analyses (Figs. 5h-5j), indicating that larger uncertainties are expected from modeled-based precipitation fields. Moreover, a study by Sheffield et al. 2013a reports that the CMIP5 models have a weak performance in representing North American climate features. Still, trend patterns from the reanalysis data (Fig. 5g) are in better agreement with the observational-based analysis. This is not surprising, as reanalysis data are generated by assimilating observations.

Mean Annual Temp-Trend 1965-2005

Annual Precip-Trend 1965-2005

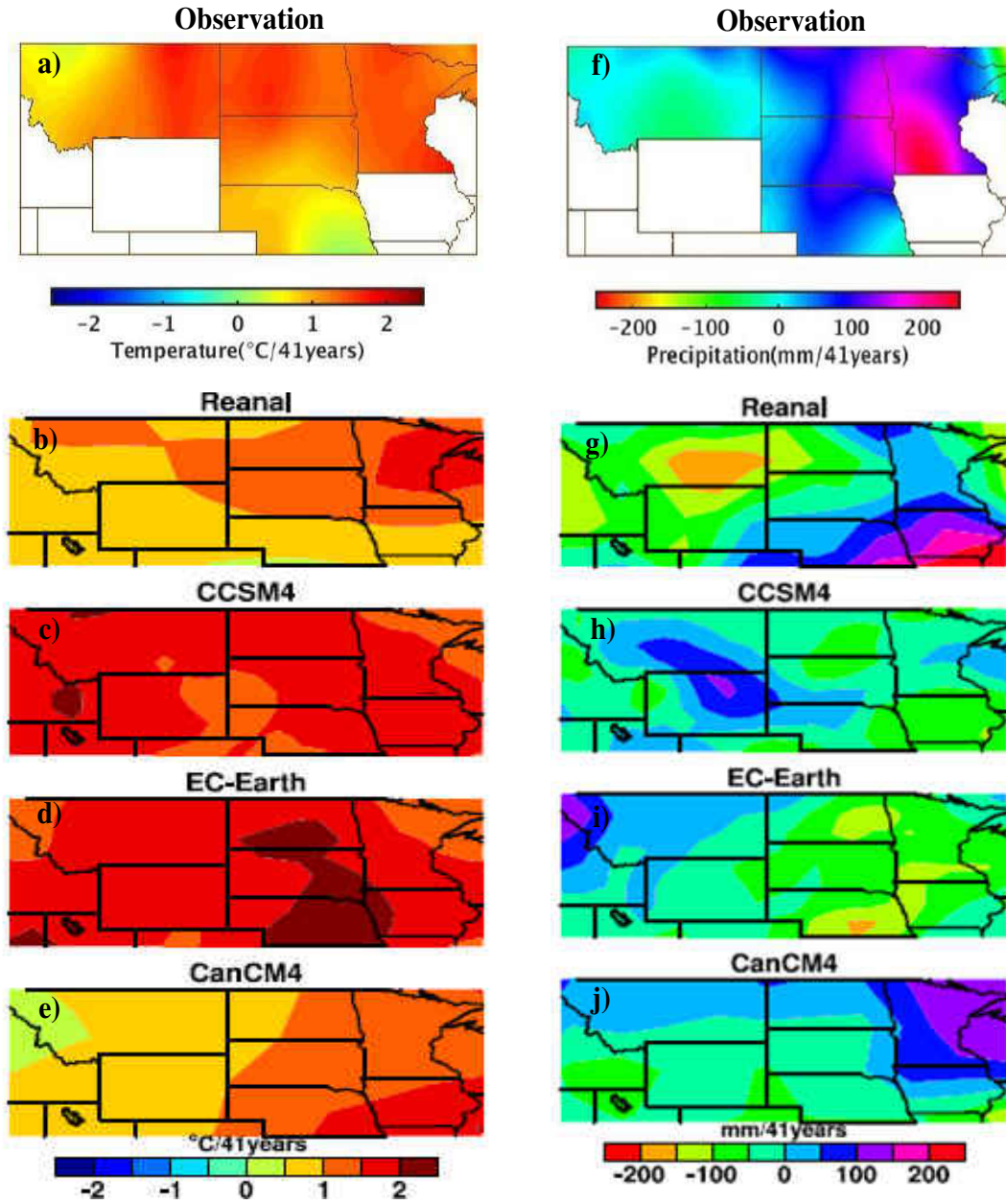


Figure 5. Long-term (left) trend (1965-2005) in temperature field for the observations (a), reanalysis (b), and model simulations (c-e). Units are in $^{\circ}\text{C}/41$ years. Long-term (right) trend (1965-2005) in precipitation field for the observations (f), reanalysis (g), and model simulations (h-j) is also shown. Units are in $\text{mm}/41$ years.

3.1.4 Correlation between the NGP's Seasonal Climate and MEI

As suggested from Sections 3.1.1-3.1.3, temperature and precipitation fields from the reanalysis data are in a closer match to observations. Thus, the reanalysis data are used for comparison with model simulations from hereafter. Also, model simulations from the three GCM runs are used to obtain ensemble means of temperature and precipitation fields, which are further used in the following analysis. Using reanalysis data, the correlations between MEI and seasonal mean temperature and precipitation values for the NGP region are studied. Figure 6 shows the spatial patterns of correlation between the MEI index and temperature (left) and precipitation (right) fields. The spatial distribution of correlation (Fig. 6a) between the MEI and Dec-Jan-Feb (DJF) temperature is positive with a correlation coefficient of 0.25 to 0.5 across North Dakota and Minnesota. This observed positive correlation between ENSO and winter temperature is also consistent with findings from Bunkers et al. (1996). Also, a study by Higgins et al. (2001) demonstrated the strong correlation between the US winter temperature extremes and interannual climate variability. Positive correlations are also found, although with lower values, between the MEI and Mar-Apr-May (MAM) (Fig. 6c) temperature. Weaker negative correlations are found between the MEI and temperature fields from the other two seasons, indicating a plausible association with La-Niña events. This suggests that impacts of ENSO have a strong influence on the NGP's seasonal temperature fields. In contrast to the temperature field, much stronger positive correlations of 0.25-0.75 are found between the MEI and summer precipitation (Fig. 6f) of the NGP region. The

correlations are much weaker for other seasons. Also, strong correlations seem to occur over regions with high annual mean cumulative precipitation.

MEI Correlation 1965-2005

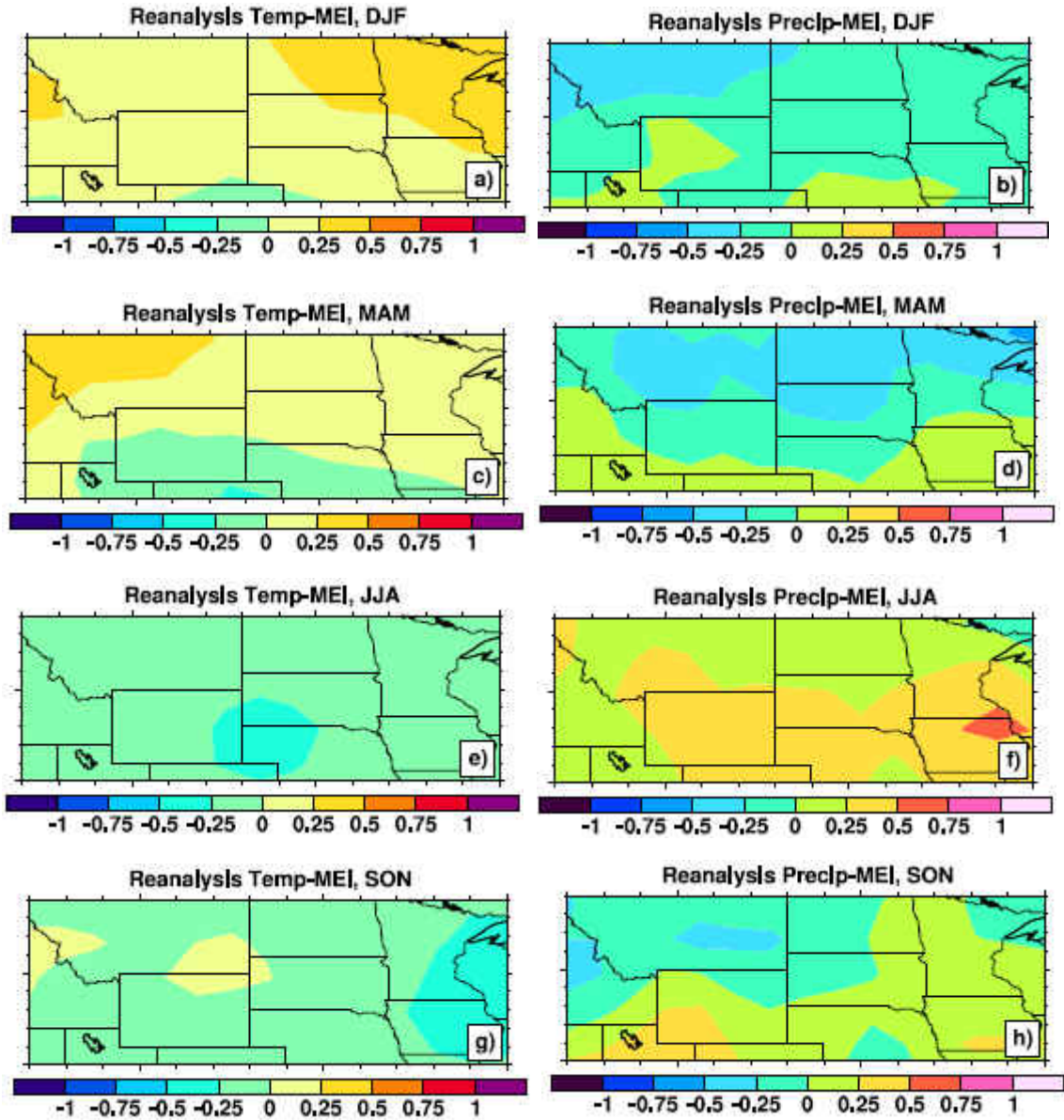


Figure 6. Spatial distribution of correlation between MEI and temperature (left) precipitation (right) for all four seasons.

CHAPTER IV

INVESTIGATION OF SEASONAL CLIMATE VARIABILITY ACROSS THE NGP THROUGH EOF ANALYSIS

Results from the heterogeneous correlation analysis of NGP's seasonal means with MEI index (Fig. 6) imply that some portion of the seasonal variabilities in temperature and precipitation of the region are likely associated with ENSO. In this section, similar investigations as shown in Chapter 3 are explained through an EOF analysis, using both detrended and non-detrended data. As described in Chapter 2, an EOF analysis is applied to the deseasonalized (anomalies) seasonal-based reanalysis data and ensemble means of the three GCM model simulations. Spatial EOF patterns (orthogonal spatially) are derived by computing eigenvectors of the covariance matrix of the data fields and temporal PC patterns (orthogonal temporally) are estimated by projecting EOF patterns onto the corresponding temperature or precipitation anomalies of original data. As a verification of EOF analysis, the derived EOFs and PCs are also examined for their orthogonality.

4.1.1. Prominent Patterns for the Temperature Field

The three leading modes of variability inherent to the respective data are derived by regressing the non-detrended seasonal anomalies (contain temporal patterns) upon the three leading standardized (normalized) PCs. The regression maps have a similar structure as the EOFs, yet with a unit of original data per standard deviation (e.g., Wang and Ting 2000; Hurrell et al. 2003; Krishnamurthy and Krishnamurthy 2013). The anomalies represent deviations from the long-term means. In general, a positive anomaly means a warmer or wetter than the normal condition and vice versa for the negative anomalies.

Figure 7 shows the regression maps of surface temperature from the EOF analysis for boreal winter (DJF) reanalysis (left panel) and CMIP5 (right panel). The percentage of variance explained by each EOF mode is also labeled on the top of each panel. As suggested in Fig. 7, the temperature field has positive anomalies over the NGP for both the model and reanalysis simulations. Note that the EOF trends should be interpreted with caution by considering both the spatial and associated temporal patterns (e.g., Section 4.1.3). From reanalysis EOF mode 1, it can be predicted that the DJF season may result in a 1-2 °C per standard deviation positive anomaly in temperature while model (ensemble) EOF 1 results in a 0.8-1.2 °C per standard deviation positive anomaly in temperature. Reasonable similarities are observed between the model (ensemble) and reanalysis spatial patterns in mode 1. Also, the percentage of variance explained by the first three modes of the reanalysis and model simulations is in the same range. It is worth noting that the observed above-normal winter seasonal variabilities across North Dakota

are consistent with the results of maximum variabilities across the same region for the annual mean (Fig. 2, right column). The major patterns explained by each EOF are different. Notable major warming patterns have been detected and explained by the first mode of variability for both simulations. Similar spatial patterns are not found between the reanalysis and the model with modes 2 and 3. Still, caution is needed while interpreting results from the EOF analysis, as uncertainties in the datasets as well as other factors could impact the results of the EOF analysis. For example, larger uncertainties are expected from the GCM-modeled precipitation fields as indicated in Chapter 3. Thus, it is likely that EOF patterns of the precipitation field may partially be affected by uncertainties in the data. Thus, the derived EOF/PC patterns may not necessarily be related to the real physical qualities (e.g., Torralba et al. 2015). The same argument is applicable throughout the EOF analysis of this study.

From Fig. 8, the reanalysis patterns for the spring (MAM) season exhibit both cooling and warming patterns, while the model patterns exhibit above-normal positive anomalies over the NGP in mode 1. Also, modes 2 and 3 of the reanalysis and model patterns are rather different. This may be related to limitations in the EOF analysis that are discussed later in this section. Also, mode 3 of the model did not satisfy the North test, indicating that the eigenvalue is not unique and thus the mode 3 patterns can be ignored. It can be inferred from both the winter and spring EOF patterns that the observed regions of maximum variability are consistent with the regions of maximum variability shown in Fig. 2 (right column).

For the summer season (Fig. 9), EOF mode 1 shows minor trends for both the reanalysis and model data, indicating no significant warming/cooling patterns for this season. EOFs 2 and 3 of both the model and reanalysis are not identical. However, EOF 3 of the reanalysis can be ignored because of the failure of the North test. For the autumn (SON, Fig. 10) season, in EOF 1, warming patterns with 0-0.8 °C per standard deviation are found for the model, while cooling patterns with 0.4-2 °C per standard deviation are observed from the reanalysis. Again, this discrepancy in spatial patterns may be due to the difference between model and reanalysis data, but may also be related to the manner in which the EOF patterns are interpreted, which is discussed later. Similar patterns are observed between the model and reanalysis for modes 2 and 3, however, they are not significant.

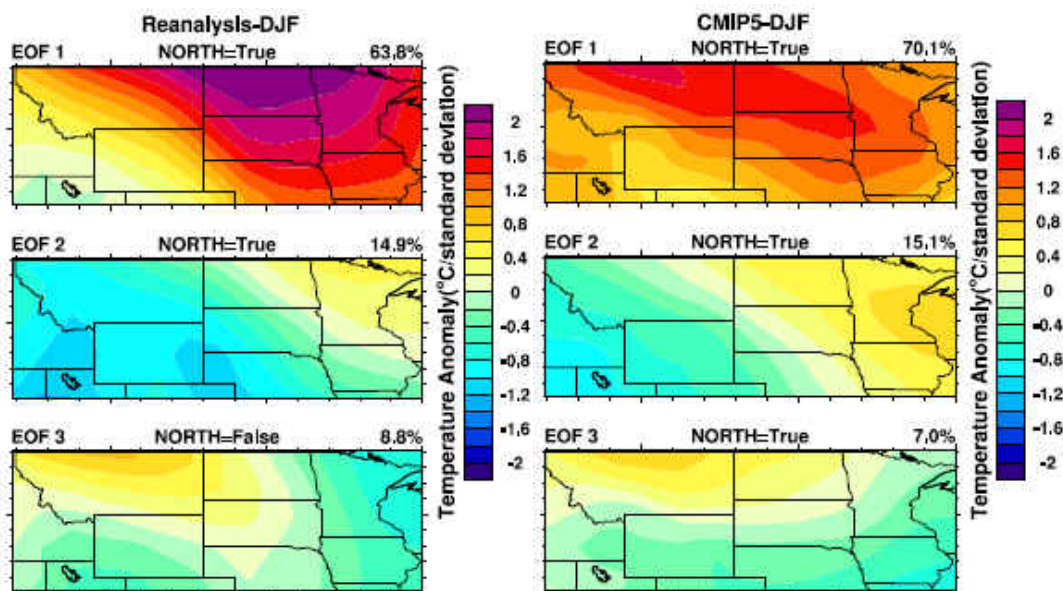


Figure 7. Regression of winter temperature anomalies onto associated three leading PCs: reanalysis (left) and model (right). The fractional variance explained by each mode is displayed in each panel's title. Units are in °C/standard deviation.

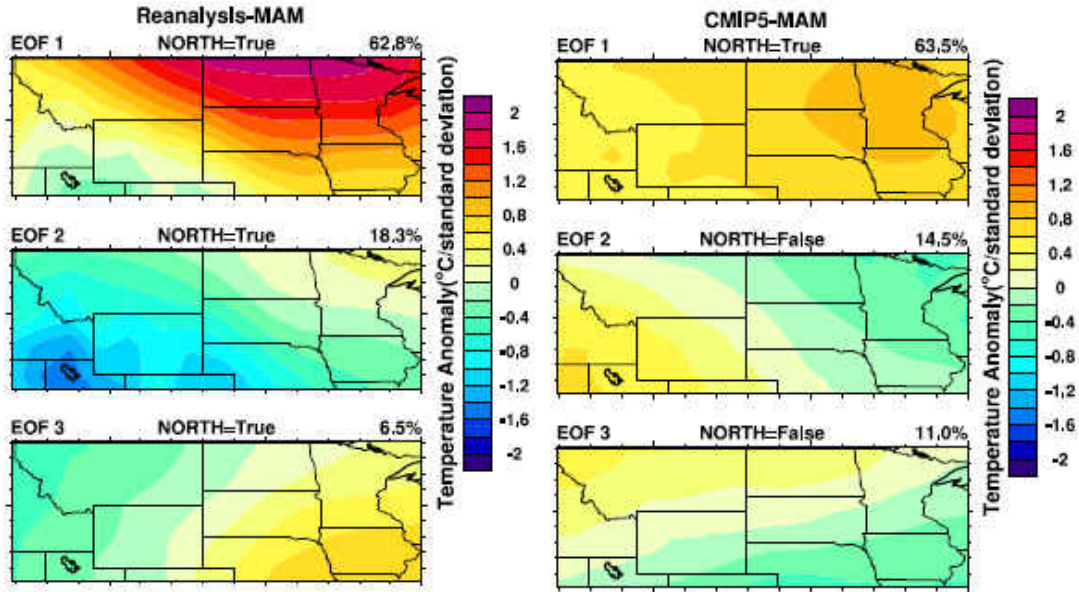


Figure 8. Regression of spring temperature anomalies onto associated three leading PCs: reanalysis (left) and model (right). The fractional variance explained by each mode is displayed in each panel's title. Units are in $^{\circ}\text{C}/\text{standard deviation}$.

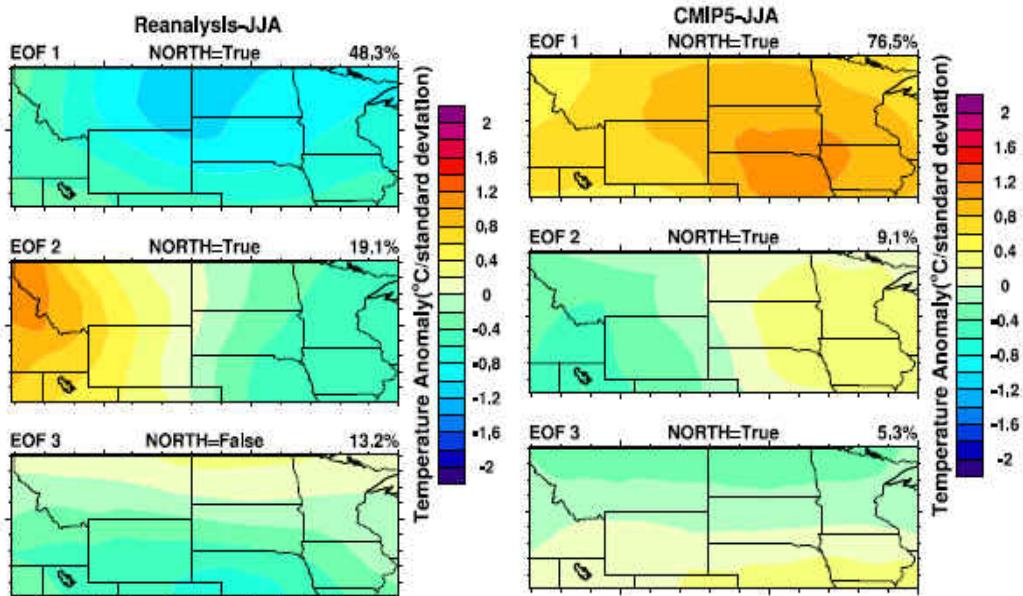


Figure 9. Regression of summer temperature anomalies onto associated three leading PCs: reanalysis (left) and model (right). The fractional variance explained by each mode is displayed in each panel's title. Units are in $^{\circ}\text{C}/\text{standard deviation}$.

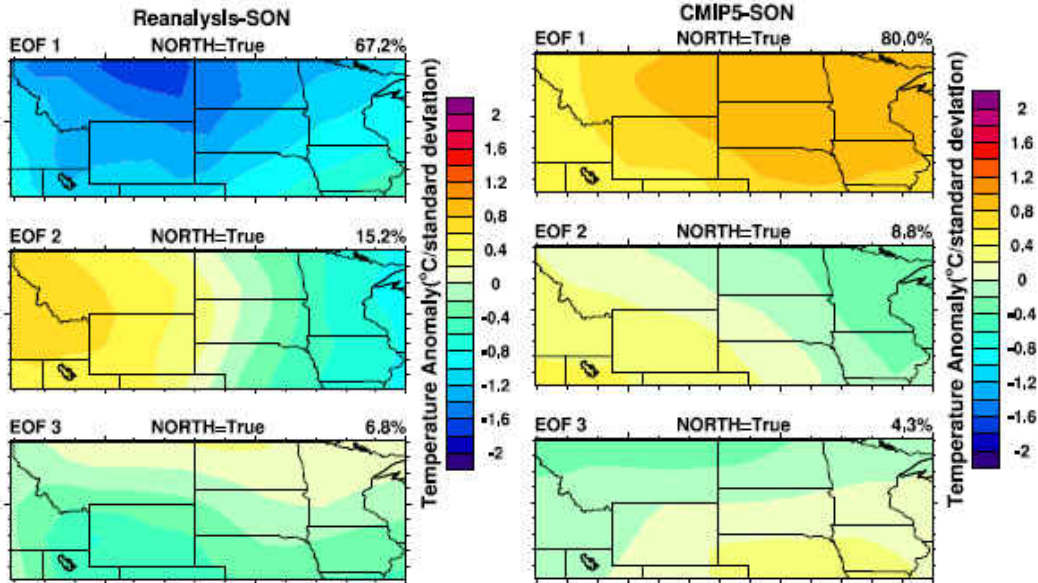


Figure 10. Regression of autumn temperature anomalies onto associated three leading PCs: reanalysis (left) and model (right). The fractional variance explained by each mode is displayed in each panel's title. Units are in $^{\circ}\text{C}/\text{standard deviation}$.

4.1.2. Prominent Patterns for the Precipitation Field

The classified structure with negative anomalies corresponds to dry-weather patterns, while the classified region with positive anomalies corresponds to regions that are wetter than normal. For the winter season (Fig. 11, DJF), below normal precipitation anomalies are observed in both the model and reanalysis, but are small in magnitude in general. Also, the dominant patterns of variability that are observed in mode 3 for reanalysis are not distinct since the North test is not satisfied, and thus the eigenvalue of mode 3 is not trustworthy.

For the spring season (MAM, Fig. 12), both positive and negative anomalies are found in the reanalysis in mode 1. The precipitation anomalies observed for the model are inconsistent with those from the reanalysis. Note that the same exercise has also been

conducted with the de-trended data, yet the patterns are totally different for the MAM season alone. This again reinforces our concern that caution is needed to interpret detected features from the EOF analysis. Also, the patterns for modes 2 (model) and 3 (reanalysis) cannot be trusted because the EOFs are not distinct.

For the summer season (JJA, Fig. 13), the positive anomalies found in the reanalysis indicate above-normal precipitation anomalies and significantly wet weather patterns in mode 1. Both the EOF and PC show a positive sign, and thus the above normal precipitation anomalies for this season are likely trustworthy. The precipitation anomalies observed for the model are inconsistent with those from the reanalysis. The model estimates below-normal precipitation anomalies with dry weather patterns across South Dakota and Nebraska in mode 1, while the reanalysis suggests significant wet conditions across the region. Still, this may also be related to how the EOFs are interpreted (discussed later). In addition, patterns from modes 2 and 3 of the reanalysis are not trustworthy, while the same modes of model data predict below-normal anomalies across the NGP.

During the autumn (SON), as shown in Fig. 14, wetter than normal patterns are observed over the eastern portion of the NGP for both the model and reanalysis. Combined with discussions in Section 4.1.3, it can be expected (i.e., EOF 1) that the NGP region is likely to be wetter than normal in autumn, but EOF 2 from the model and reanalysis contradicts the EOF 1 results with less major dominant patterns. Modes 2 and 3 of reanalysis and model patterns are not trustable due to the failure of the North test (i.e., EOFs 2 and 3). Relatively similar patterns of variability are observed for both the model and reanalysis for the winter and autumn seasons.

Overall, the model results contradict the reanalysis for the precipitation field. In mode 1, major anomalous wet patterns are found in the summer and autumn seasons for the reanalysis, yet the model predicts negative anomalies in summer. Still, it is compelling that the regions of maximum variability observed in Fig. 3 are consistent with the regions of highest variance found for the summer and autumn seasons in mode 1, especially across Nebraska. Still, Figs. 11-14 suggest that there might be large uncertainties in model-simulated precipitation and thus the modeled precipitation fields may be less trustable. Figs. 11-14 also suggest that extra caution is needed to interpret trends from the EOF analysis.

In addition, there is no significant linear relationship between the temperature and precipitation variability (at least in the case of mode 1). The results from this precipitation analysis suggest that regions with warmer weather patterns are not experiencing heavy rainfall and floods, and precipitation seems to be not impacted by the rise in water vapor and evaporation associated with warmer temperatures. Thus, the patterns of temperature and precipitation are not highly correlated. These results of seasonal climate variabilities are in good agreement with findings from the previous sections.

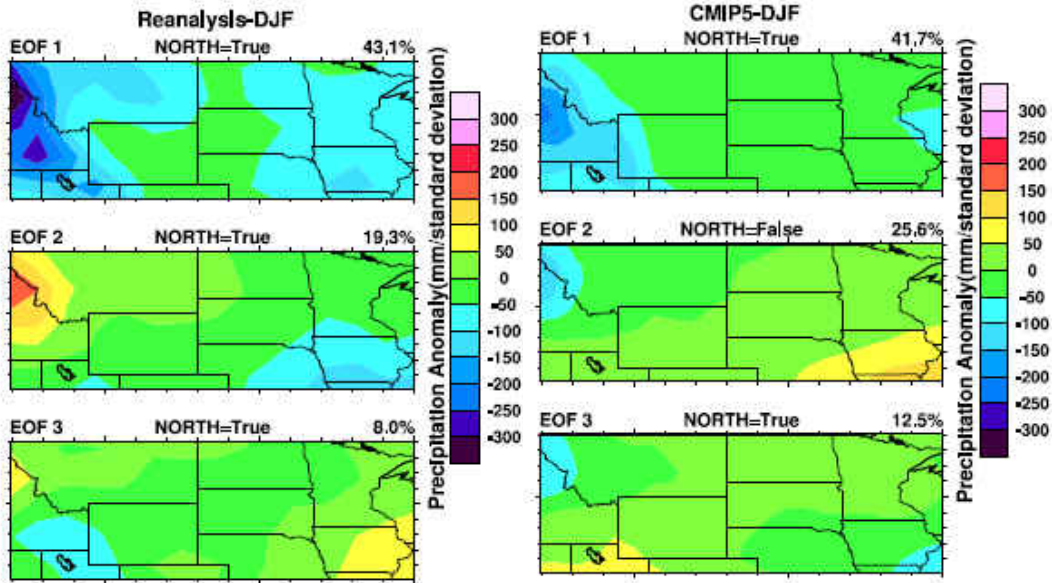


Figure 11. Regression of winter precipitation anomalies onto associated three leading PCs: reanalysis (left) and model (right). The fractional variance explained by each mode is displayed in each panel's title. Units are in mm/standard deviation.

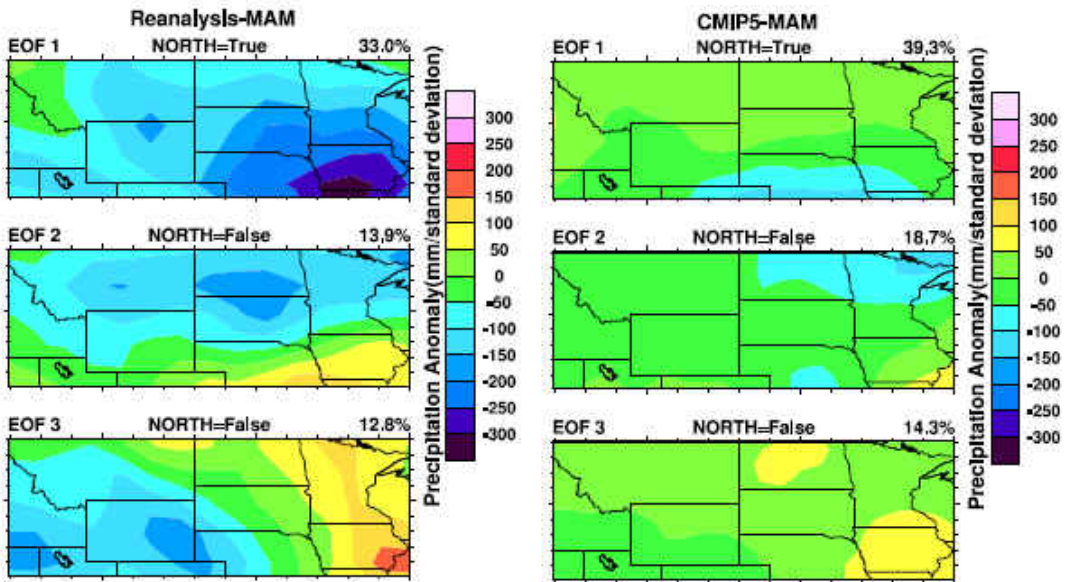


Figure 12. Regression of spring precipitation anomalies onto associated three leading PCs: reanalysis (left) and model (right). The fractional variance explained by each mode is displayed in each panel's title. Units are in mm/standard deviation.

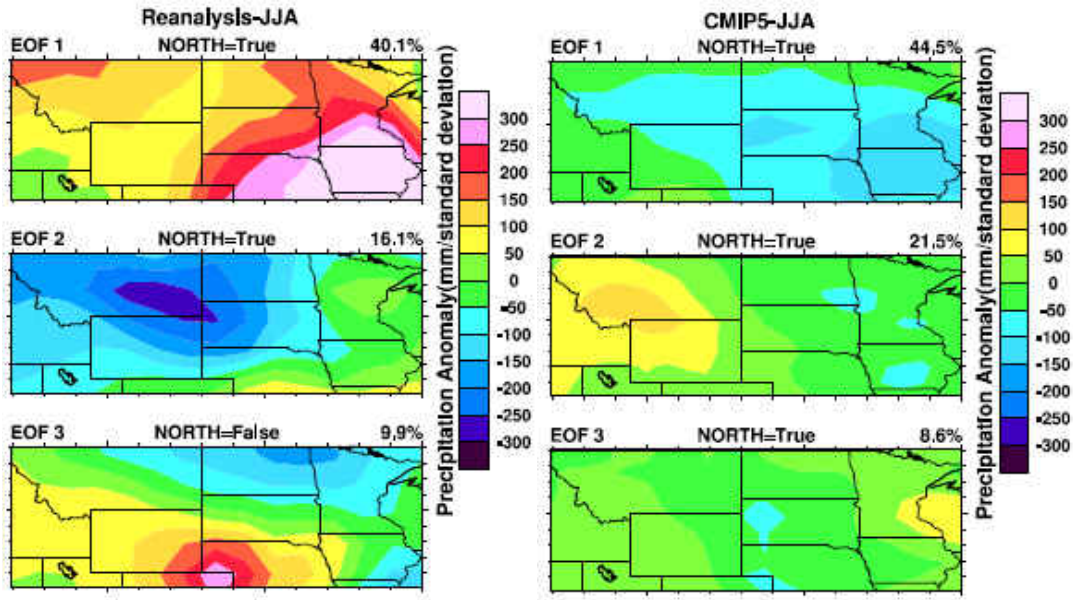


Figure 13. Regression of summer precipitation anomalies onto associated three leading PCs: reanalysis (left) and model (right). The fractional variance explained by each mode is displayed in each panel's title. Units are in mm/standard deviation.

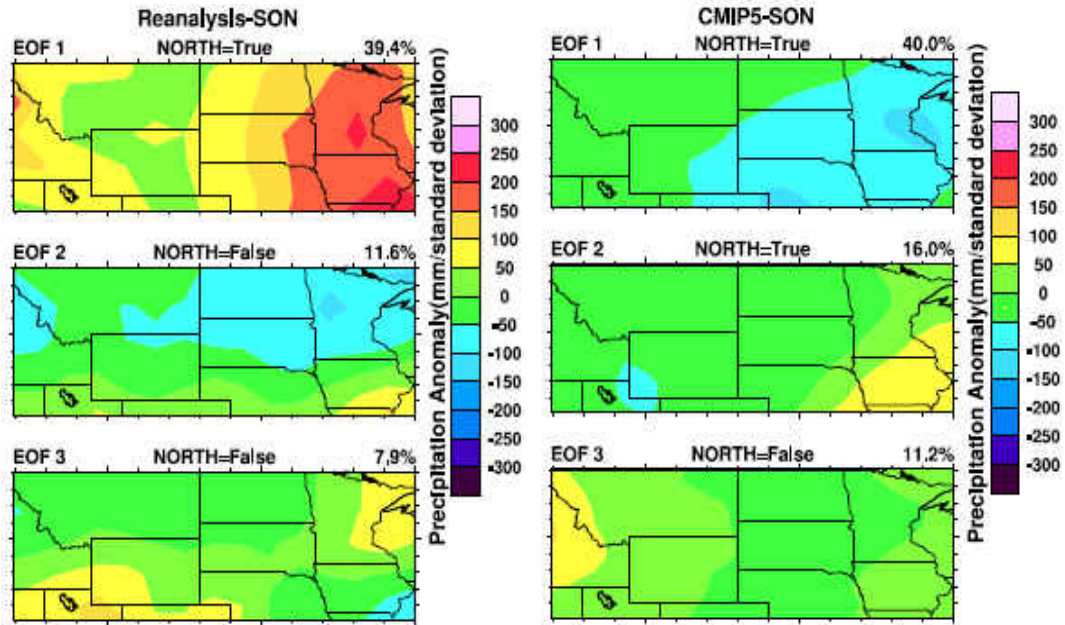


Figure 14. Regression of autumn precipitation anomalies onto associated three leading PCs: reanalysis (left) and model (right). The fractional variance explained by each mode is displayed in each panel's title. Units are in mm/standard deviation.

4.1.3 Seasonal Trend Analyses and Potential Issues

In this section, non-detrended data are used to study the temporal patterns of seasonal temperature and precipitation trends of the NGP region. It is also interesting to compare temporal trends estimated using raw reanalysis data as well as from the EOF analysis (PC1), as shown in Fig. 15. The regionally-averaged temperature time series pattern estimated from raw data is in phase with PC1 for the DJF (Fig. 15a) and MAM (Fig. 15c) seasons. However, the temporal patterns are almost identical between raw reanalysis and PC1 but out of phase with each other for the JJA (Fig. 15e) and SON (Fig. 15g) seasons. In fact, it seems that by multiplying -1 to the PC1 patterns, they are again remarkably similar to the temperature trends estimated from the raw reanalysis data. For the precipitation field, almost identical time series patterns are found between the PC1 and raw-data based estimations for the JJA (Fig. 15f) and SON (Fig. 15h) seasons. Yet, for the DJF (Fig. 15b) and MAM (Fig. 15d) seasons, the temporal patterns seem completely out of phase.

In addition, while the EOF analysis is implemented using the NCL language, similar steps are repeated with the use of the IDL programming language for sanity check purposes. Again, for the temperature field, PC1 patterns are identical for the DJF, MAM, and SON seasons. The PC1 pattern is similar for the JJA season, but is opposite in sign. This clearly indicates that the arbitrary nature of sign in EOF analysis (Dennis L. Hartmann 2016). This practice suggests that caution is needed while using EOF for trend analysis. In fact, this issue is also documented in the UCAR NCL webpage (<http://www.ncl.ucar.edu/Document/Functions/Built-in/eofunc.shtml>) as follows:

“EOFs are eigenvectors of the covariance matrix formed from the input data. Since an eigenvector can be multiplied by any scalar and still remain an eigenvector, the sign is arbitrary. In a mathematical sense, the sign of an eigenvector is rather unimportant. This is why the EOF analysis may yield different signed EOFs for slightly different inputs. Sign only becomes an issue when you wish to interpret the physical meaning (if any) of an eigenvector.”

“You should approach the interpretation of EOFs by looking at both the EOF pattern and the associated time series together. For example, consider an EOF of sea surface temperature. If your EOF has a positive centre and the associated time series is increasing, then you will interpret this centre as a warming signal. If your EOF had come out the other sign (ie. a negative centre), then the associated time series would also be the opposite sign and you would still interpret the centre as a warming signal.”

Nevertheless, Fig. 15 confirms that temporal trends in temperature and precipitation have a seasonal dependence. For example, a $\sim 1\text{-}2$ °C per 41 years increase is expected for the DJF season, while negligible temperature trends are found for other seasons. For the precipitation field, an increasing trend is expected for the JJA season for the NGP region, while trends from other seasons are rather marginal. However, computed trends for the wintertime temperature and summertime precipitation are not statistically significant at the 95% confidence level.

Lastly, similar processes are repeated, but with the use of the detrended reanalysis and model data. Most patterns are similar from both trended and detrended analyses, however large differences in MAM precipitation patterns are found. While the detrended

data suggests a wet pattern (not shown), the non-detrended analysis shows a dry pattern. Again, this section suggests that the patterns detected from the EOF analysis need to be carefully interpreted.

Standardized anomalies -1965-2005

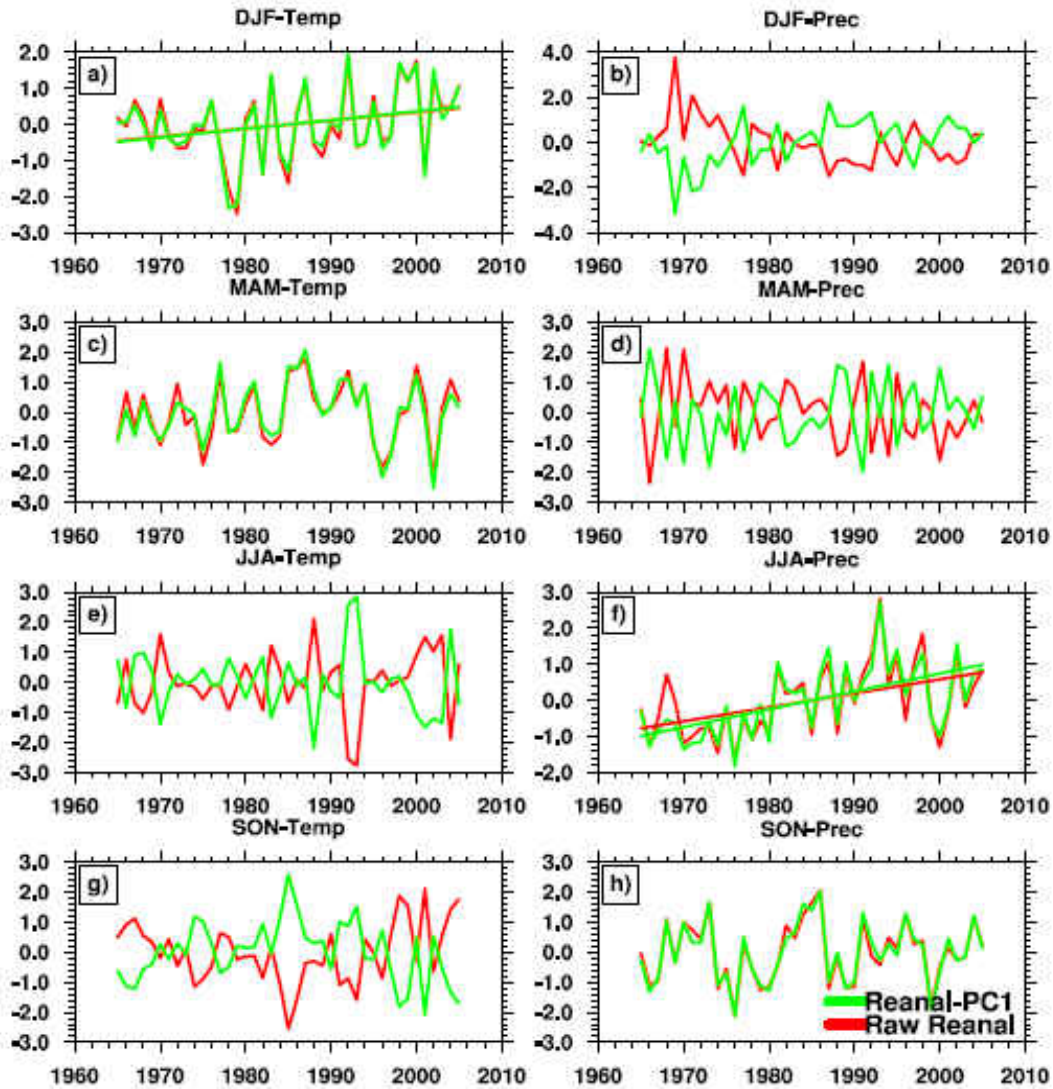


Figure 15. Normalized time series (1965-2005) of NGP's temperature (left column) and precipitation (right column). Units are in standard deviations.

4.2 Time-series Analysis between the NGP's climate variability and MEI

An advantage of PC analysis is to identify extreme events and their variations over time. In the previous section, we studied the dominant spatial patterns of temperature and precipitation as well as their temporal variations with non-detrended data. In this section, regional climate variabilities are studied with respect to an ENSO index: MEI. To achieve this goal, different from that of the previous section, de-trending is performed before the EOF analysis to remove temporal trends from the anomalies.

In addition, the relative importance of each EOF mode is determined by the fraction of the total variance that each mode explains. To express the variance information for all the observations together, the total variance explained by each dataset for all four seasons is shown in Table 1. This table illustrates that the maximum influence observed for the temperature ranges from 82% to 93%. The maximum influence observed for the precipitation field ranges from 59% to 74%. This suggests that the first three seasonal EOFs can be used to better explain variances in NGP's temperature than precipitation fields, which is consistent with what was reported in Wang et. al (2012).

As the next step, the EOF-based temperature and precipitation analyses are correlated with an ENSO index (MEI). For illustration purposes, Table 2 shows the warm and cold ENSO events that were compiled by Golden Gate Weather Services for the period of 1965-2005 (Huang et al. 2015).

Table 1. Percentage of the total variance explained by the first three seasonal EOFs.

	Temperature		Precipitation	
	CMIP5	Reanalysis	CMIP5	Reanalysis
DJF	91%	88%	78%	70%
MAM	88%	88%	63%	63%
JJA	87%	82%	68%	78%
SON	93%	91%	70%	61%

Table 2. El-Niño and La-Niña events for the period of 1965-2005 (acquired from <http://ggweather.com/enso/oni.htm>).

	El-Niño MEI Events			La-Niña MEI Events			
	Moderate	Strong	Very Strong	Weak	Moderate	Strong	Weak
1986-87		1965-66	1982-83	1968-69	1970-71	1973-74	1967-68
1987-88		1972-73	1997-98	1969-70	1998-99	1975-76	1971-72
1991-92				1976-77	1999-00	1988-89	1974-75
2002-03				1977-78			1983-84
				1979-80			1984-85
				1994-95			1995-96
				2004-05			2000-01

Table 3. Correlations between the first three EOF coefficient time series (1965-2005) and the MEI sequence of winter, spring, summer, and autumn when using the CMIP5 model, and reanalysis (a) surface temperature, (b) precipitation anomalies. Variances that correspond to each mode are displayed in parentheses beside the correlation coefficient. Correlation coefficients that exhibit a 95% significance level are highlighted in bold.

a)

Temperature	PC1 & MEI		PC2 & MEI		PC3 & MEI	
	CMIP5	Reanalysis	CMIP5	Reanalysis	CMIP5	Reanalysis
DJF	-0.07 (63%)	0.23 (61%)	0.20 (19%)	0.15(20%)	-0.003(9%)	-0.02 (8%)
MAM	-0.10 (60%)	0.16 (55%)	0.17 (17%)	0.12(25%)	-0.13(12%)	0.41 (8%)
JJA	0.23 (67%)	0.25 (47%)	-0.005(13%)	-0.01(23%)	0.03 (7%)	0.06 (13%)
SON	0.04 (80%)	0.11 (69%)	-0.01 (8%)	0.22 (16%)	0.18 (5%)	-0.05 (6%)

b)

<u>Precipitation</u>	PC1 & MEI		PC2 & MEI		PC3 & MEI	
	CMIP5	Reanalysis	CMIP5	Reanalysis	CMIP5	Reanalysis
DJF	0.08 (46%)	0.20 (44%)	0.05 (22%)	-0.21 (17%)	0.09(10%)	-0.38(9%)
MAM	0.20 (32%)	0.07 (40%)	-0.40 (20%)	-0.08 (14.3%)	-0.11(11%)	0.40(9%)
JJA	-0.09 (43%)	0.38 (50%)	0.09 (17%)	0.31(16%)	0.09(9%)	-0.10(12%)
SON	-0.24 (42%)	-0.007 (40%)	0.01 (15%)	0.11(11%)	-0.23(13%)	-0.10(10%)

To examine the variation in temperature and precipitation associated with the ENSO events, time series plots of the standardized anomalies of modes 1, 2, and 3 are shown in

Figs. 16 and 17. These results are also shown in Table 3, which includes the MEI correlation coefficients with three leading principal components of surface temperature and precipitation anomalies.

For the winter season (Fig. 16, left column, and Tables 2 and 3), there is a well-defined, quasi-linear, in-phase or out-of-phase relationship between all variables and the El-Niño events. Here “in-phase” is defined as both variables having similar temporal patterns and “out-of-phase” is defined as the temporal patterns of both variables being similar but opposite in sign. Note that the signs of EOFs are rather arbitrary as shown from the previous section, and thus both in- and out-of-phase of MEI with PC modes are considered related in this study. In winter, the consistent in/out -of-phase fluctuations of the PC1 time series with MEI clearly indicate a potential linkage between the NGP’s winter temperature and the ENSO events. The reanalysis temperature is in-phase with the major El-Niño (Table 2) events (1982-83, 1986-87, 1991-1992, and 1997-98). The model temperature is in-phase with the 2002-2003 moderate El-Niño event. These results suggest that the El-Niño events might be one of the causes of the observed major warming patterns in the same season (Fig. 7) across North Dakota and Montana. The corresponding precipitation patterns (Fig. 17, left column, and Tables 2 and 3) do also reflect some consistent in/out -of-phase fluctuations with ENSO events. Between 1972-1980, excess dry and wet precipitation patterns are observed in both reanalysis and model. However, computed correlation coefficients do not reflect any significant connection with ENSO (Tables 3a and 3b).

In the spring (Figs. 16 and 17 left columns, and Table 3), there is no consistent in/out of phase fluctuation between each variable and MEI for both the simulations, but a notable shift exists between all simulations associated with ENSO events in the temperature field. The consistent time series patterns between model and reanalysis are found for both simulations from 1965-1985 for the temperature field. Both the model and reanalysis precipitation fields are in-phase with the 1982-83 and 1997-98 strong El-Niño events. However, insignificant correlation coefficients are found for both temperature and precipitation fields in association with ENSO.

During the summer, there is no consistent in/out -of-phase fluctuation with MEI for the temperature field (Fig. 16, left column). The reanalysis precipitation (Fig. 17, left column) field displays a coherent pattern with a strong significant positive correlation coefficient of 0.38. However, a significant correlation coefficient is not found for the model with MEI. Both reanalysis (in) and (out) model precipitation fields are in-phase with the major El-Niño events (2002-2003).

In autumn (Figs. 16 and 17, left column, and Table 3), none of the variables and simulations have consistent in/out -of-phase fluctuations associated with ENSO. Also, no significant correlation is observed between all datasets and MEI index. Overall, it can be deduced from the mode 1 reanalysis time series that ENSO tends to accompany prominent winter temperature and summer precipitation patterns across the NGP. These results are in agreement with previous results from this study.

The analyses for EOF and PC modes 2 and 3 are also included in Figs. 16 and 17, as well as Table 3. Since EOF modes 2 and 3 contain less information as EOF mode 1,

only significant findings are discussed here. For example, for the EOF 2 and PC 2 analysis, in the spring season, there are consistent fluctuations with significant negative correlation coefficients of 0.40 for precipitation (CMIP5). The significant negative correlation found for the precipitation field can be associated with the observed dry weather with weak loadings in mode 2 across North Dakota (Fig. 12; right). For the EOF 3 and PC 3 analysis, in the spring season, a significant and coherent positive correlation was observed in reanalysis for both fields. The significant positive correlation coefficient of 0.41 is found between temperature and MEI for the same mode and season. For precipitation, a significant correlation coefficient of 0.40 is observed. Moreover, the results reveal uncertainties between the CMIP5 and reanalysis simulations. Also, results from the time series analysis are consistent with results from the spatial patterns (Figs. 7-14) of maximum variability for all seasons.

Standardized anomalies of temperature field

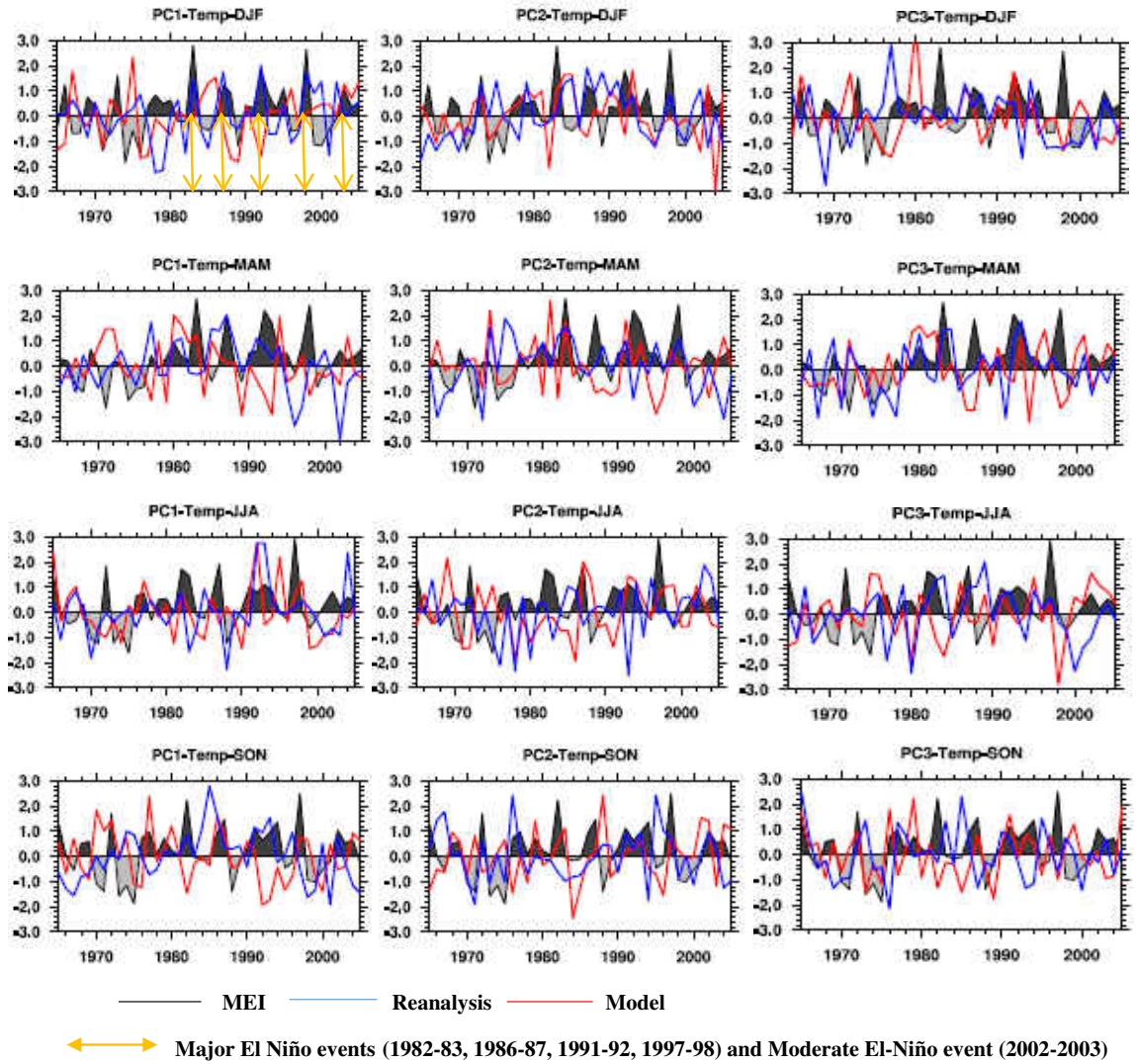


Figure 16. Normalized time series (1965-2005) of MEI and the NGP's temperature for Mode 1 (left column), Mode 2 (middle column), and Mode 3 (right column). The dark-shaded region corresponds to El-Niño events, and the light-shaded region corresponds to La-Niña events. Units are in standard deviations.

Standardized anomalies of precipitation field

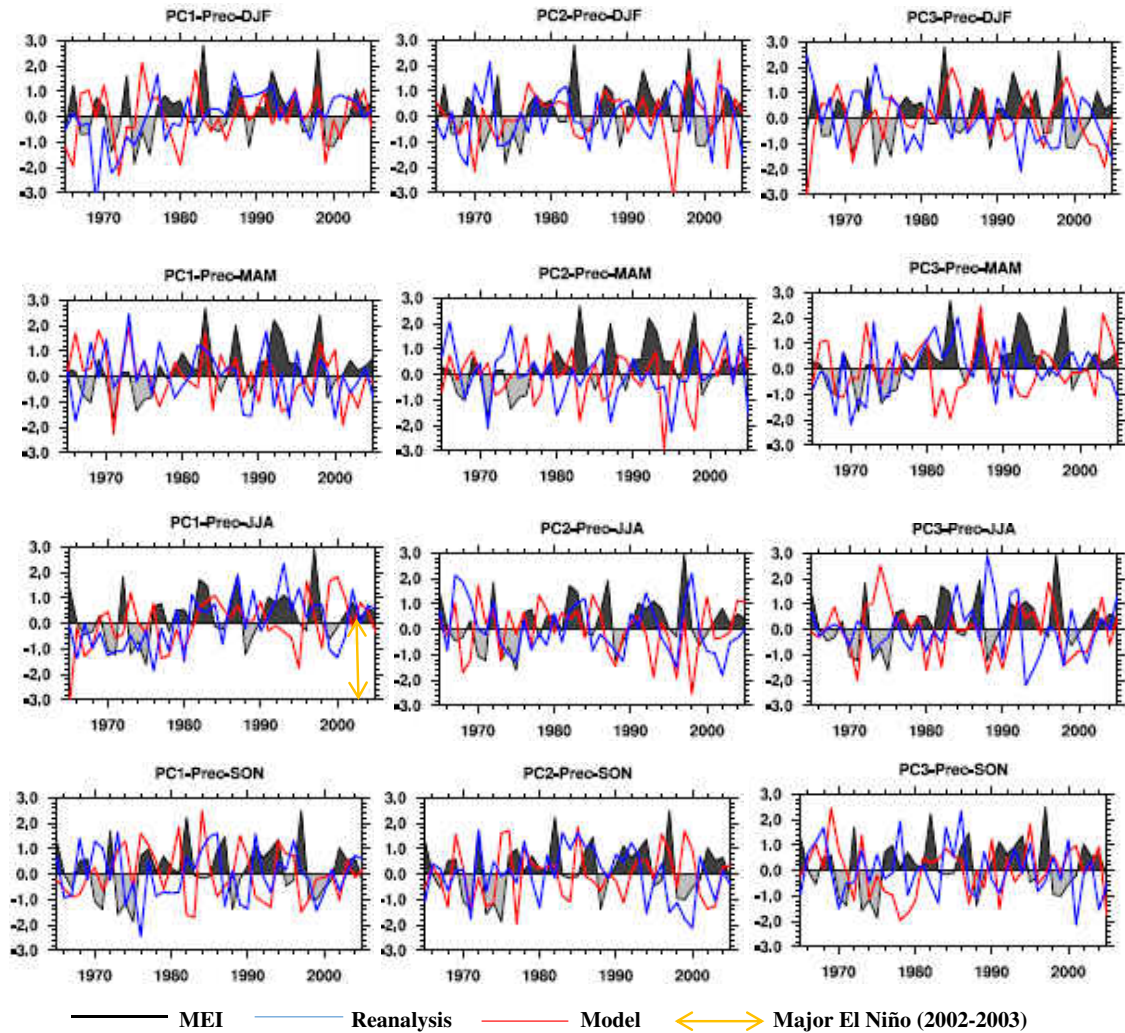


Figure 17. Normalized time series (1965-2005) of MEI and NGP's precipitation for Mode 1 (left column), Mode 2 (middle column), and Mode 3 (right column). The dark-shaded region corresponds to El-Niño events, and the light-shaded region corresponds to La-Niña events. Units are in standard deviations.

4.3 Potential Linkage of the NGP's Climate Variability (reconstructed) with the MEI Index

In this section, the linkage between MEI and the reconstructed NGP's temperature and precipitation fields are evaluated spatially. The reconstructed fields of detrended data are produced for all variables by projecting each of the three leading EOF spatial patterns on each of the associated three leading principal components. The dominant patterns for the three leading modes, along with their information, are retained in the newly reconstructed data (Smith et al. 1996). To explore the ENSO effects on the NGP with the help of a reconstructed field, heterogeneous correlation and regression maps are computed for all fields. Here, the correlation map is unitless, whereas the regression map retains the original unit of the data per standard deviation. These maps are constructed by regressing or correlating temperature or precipitation fields with the MEI index (Hartmann 2015). The regression map, which is different from the regression maps as mentioned in Section 4.1, explores the changes in the meteorological field that are linked with ENSO, and the significance of those results is explained by the correlation map (Kushnir and Wallace 1989; Taguchi and Hartmann 2006). The fundamental goal of the correlation analysis is to forecast the change in one variable with respect to fluctuations with another variable. Additionally, these maps also referred to as one-point correlation maps (Wang et al. 2012). Because EOF analysis is purely mathematical, the results from this section are also inter-compared with the results shown in Fig. 6.

4.3.1. Relationship between Temperature and MEI

The left column in Fig. 18 shows the regression maps created by regressing the reconstructed reanalysis temperature anomalies on the MEI index for all four seasons (1965-2005). Similarly, the right column in Fig. 18 shows the regression maps for the reconstructed CMIP5 temperature anomalies for all four seasons (1965-2005). These regression patterns explain the amplitude of change associated with MEI index. In the winter season (Fig. 18a), a positive temperature anomaly of 0.4-0.6 °C per standard deviation is found that is associated with El-Niño events across North Dakota. In the spring season (Fig. 18c), warming patterns associated with El-Niño events were observed across Montana, North Dakota, and Minnesota. A positive temperature anomaly of 0.3-0.5 °C per standard deviation is observed across these regions for the reanalysis data. Insignificant trends are found from the other seasons, as well as from model data. Fig. 19 presents the correlation maps that are created by correlating the temperature anomalies with MEI index for all four seasons over 1965-2005. These correlation patterns explain the significance of the association between the NGP's climate variability and MEI. The correlation patterns are, not surprisingly, almost identical to the regression patterns, except that the units are different. Similar to the regression maps (Figs. 18a & 18c), significant positive correlations are only observed for winter and spring temperature anomalies for the reanalysis data. The correlation coefficients between reanalysis winter as well as spring temperatures and MEI are ~0.3 for North Dakota and Minnesota. Again, inconsistencies are found between model and reanalysis data in both regression and correlation-based analyses. Model simulations fail to capture the teleconnection

between the MEI and NGP's climate. This might be because teleconnections between the ENSO and North American climate are poorly reproduced in CMIP5 model simulations (Sheffield et al. 2013b). It can also be inferred from Figs. 18a and 18c that ENSO exerts an influence on the winter surface temperatures across most of the NGP. Also, these findings are in good agreement with the results shown in Figs. 6, 7, and 8. These results are also in good agreement with a study by Yoden et al. (2002).

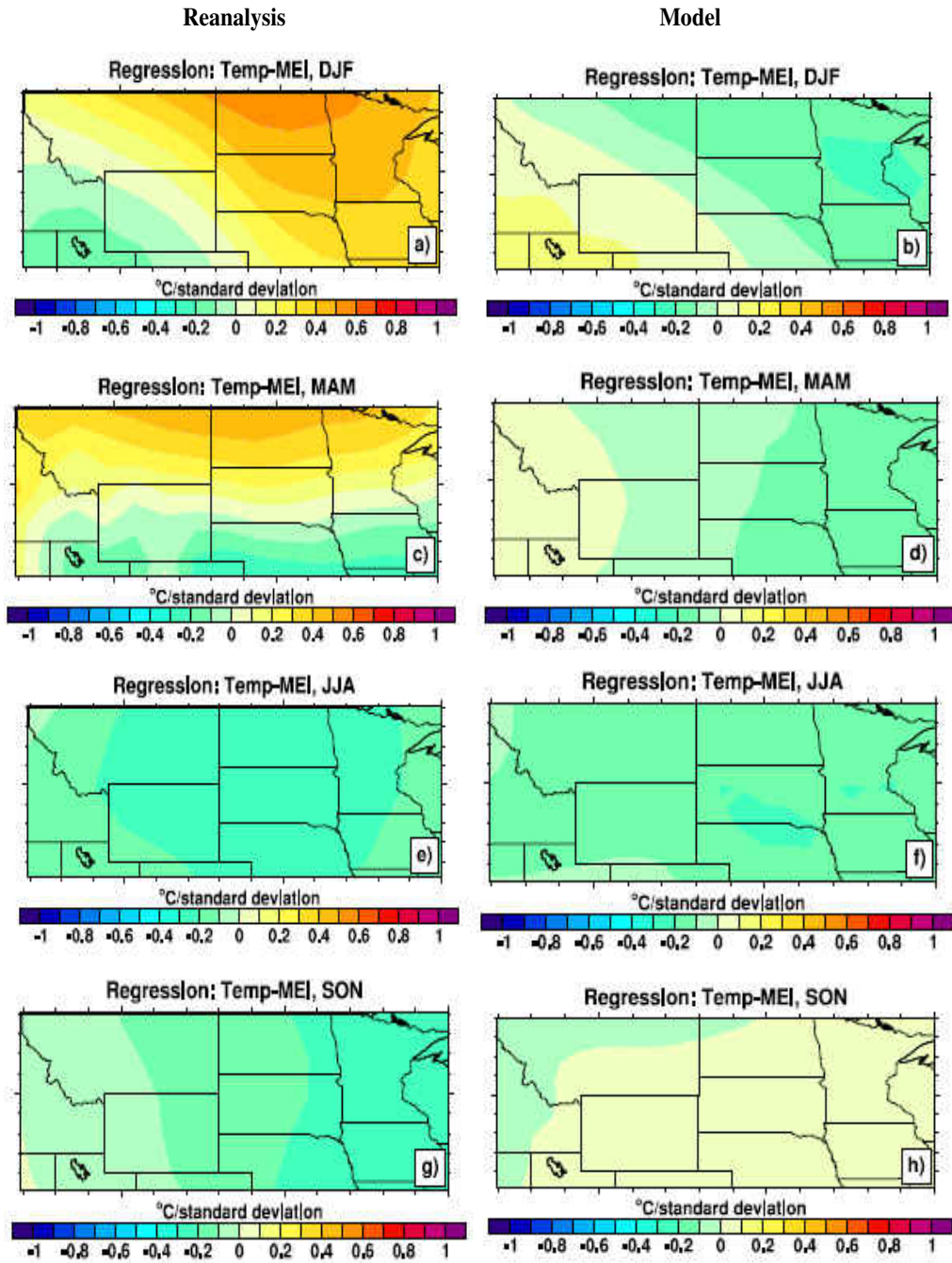


Figure 18. Regression patterns of four seasonal temperature anomalies with the MEI for 1965-2005: reanalysis (left) and model (right).

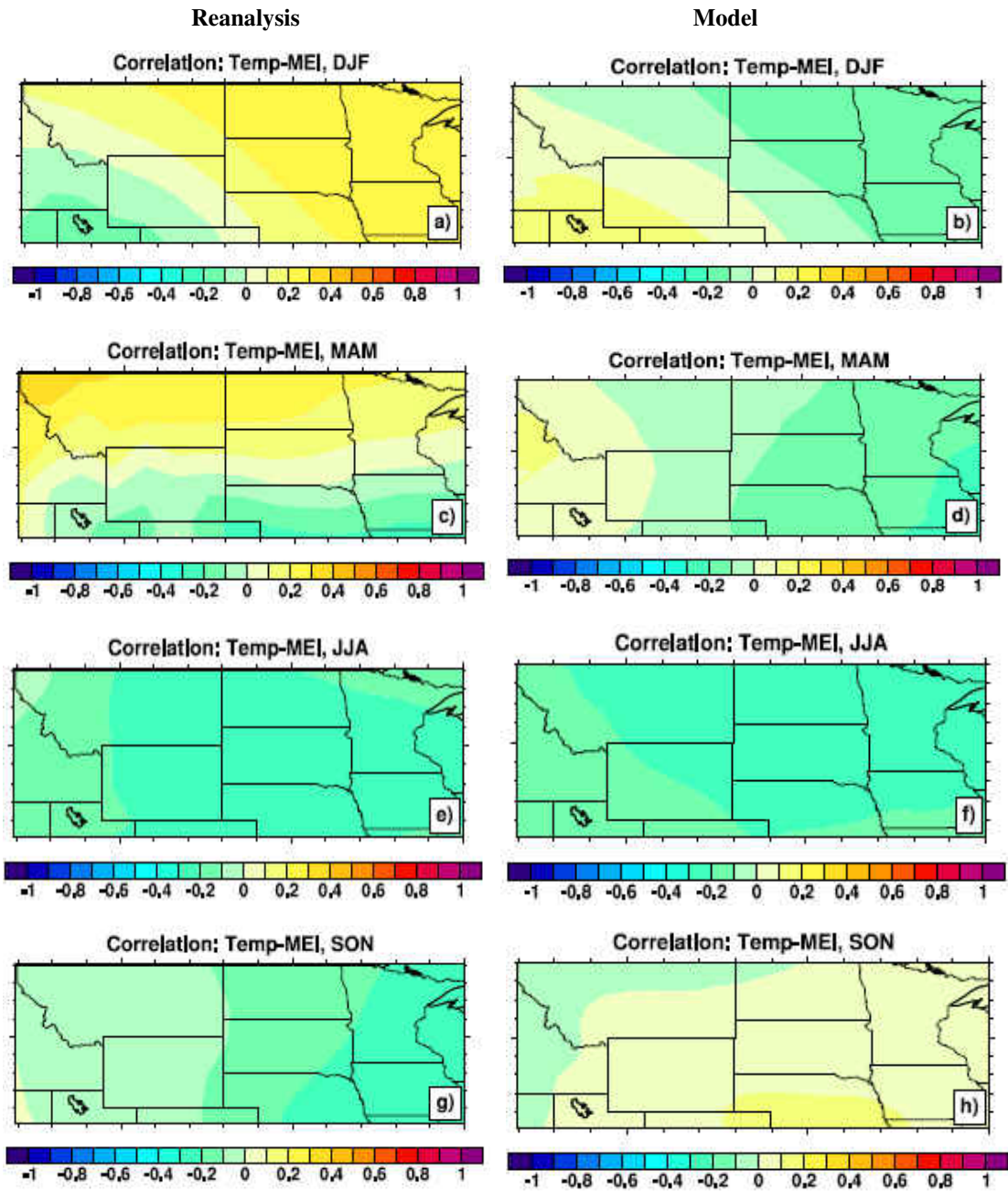


Figure 19. Correlation patterns of four seasonal temperature anomalies with the MEI for 1965-2005: reanalysis (left) and model (right).

4.3.2. Relationship between Precipitation and MEI

Fig. 20 (left column, reanalysis; right column, model) shows the regression maps produced by regressing the reconstructed reanalysis precipitation anomalies upon the MEI for all four seasons (1965-2005). These results explain the amplitude of change in association with MEI. In winter (Figs. 20a & 20b), there is no significant amplitude change observed across the NGP. However, these results are consistent with the reanalysis and model. In spring (Figs. 20c & 20d), dry patterns with below normal anomalies are observed across Montana, North Dakota, South Dakota, and Minnesota. Significant wet conditions are observed across Nebraska. These results are consistent between reanalysis and model data. Reanalysis summer regression patterns (Fig. 20e) show an anomalous precipitation pattern originates in northwest Montana and appears to progress strongly in Nebraska and the southeast part of the NGP. For summer precipitation, 50-125 mm per standard deviation change is observed in association with El-Niño events across South Dakota and Nebraska. While for the same season, model regression patterns (Fig. 20f) reflect a positive trend, though it is not significant. In the autumn season (Figs. 20g & 20h), moderate drying patterns are found across the NGP in reanalysis and model data.

The correlations of precipitation patterns associated with MEI are shown in Fig. 21 (left column, reanalysis; right column, model). In the winter season (Fig. 21a & 21b), there are no significant patterns for both reanalysis and model data. However, correlations of 0.3-0.4 are found across Montana in association with MEI. In the spring

season (Figs. 21c & 21d), dry precipitation patterns are found across the northern NGP and wet precipitation patterns across the southern NGP, as indicated by Fig. 20. Correlations of 0-0.4 are observed across Montana, North Dakota, and Minnesota for reanalysis data. But for the models, significant wet precipitation patterns with correlation coefficients of ~ 0.5 are found across Nebraska. In the summer season (Fig. 21e), significant wet conditions in association with MEI are observed across Montana, Nebraska, and South Dakota. However, there are no significant anomaly patterns using model data (Fig. 21f). In the fall season (Figs. 21g & 21h), insignificant dry conditions are observed for both model and reanalysis data, though the reanalysis patterns show correlations of 0.2-0.4 across eastern Montana. Also, for both model and reanalysis data, regression patterns are similar to the correlation patterns, as major features from the regression plots can be identified from the correlation figures. Again, no similarity is found between the precipitation (Fig. 20) and temperature (Fig. 18) patterns, as warm areas mostly do not correspond to wet areas. Results from this study indicate that the winter and spring surface temperatures, and the summer precipitation, across most of the NGP region, are likely influenced by ENSO. Also, Fig. 20 seems to suggest a rather large uncertainty in the modeled precipitation fields, similar to previous discussions.

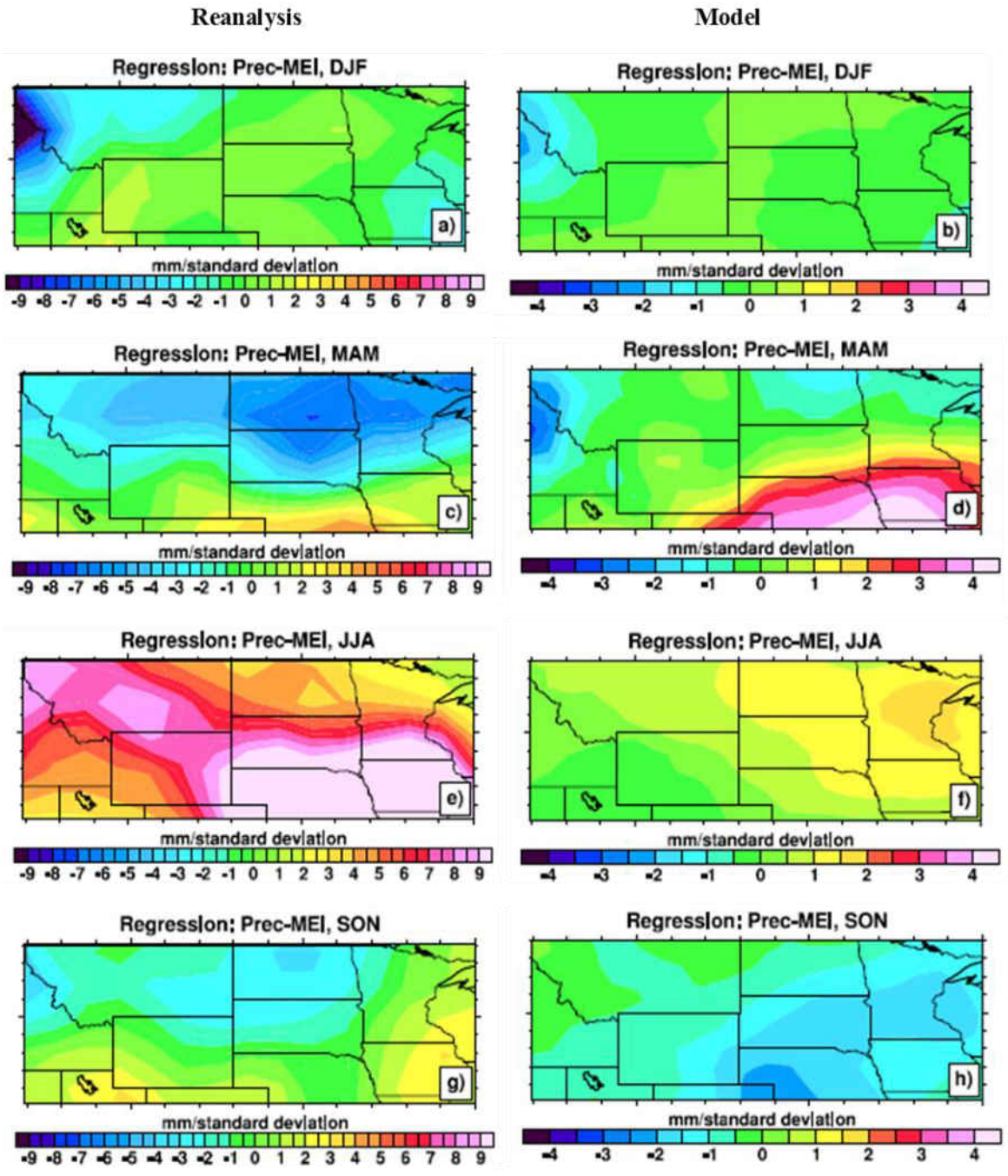


Figure 20. Regression patterns of four seasonal precipitation anomalies with the MEI for 1965-2005: reanalysis (left) and model (right).

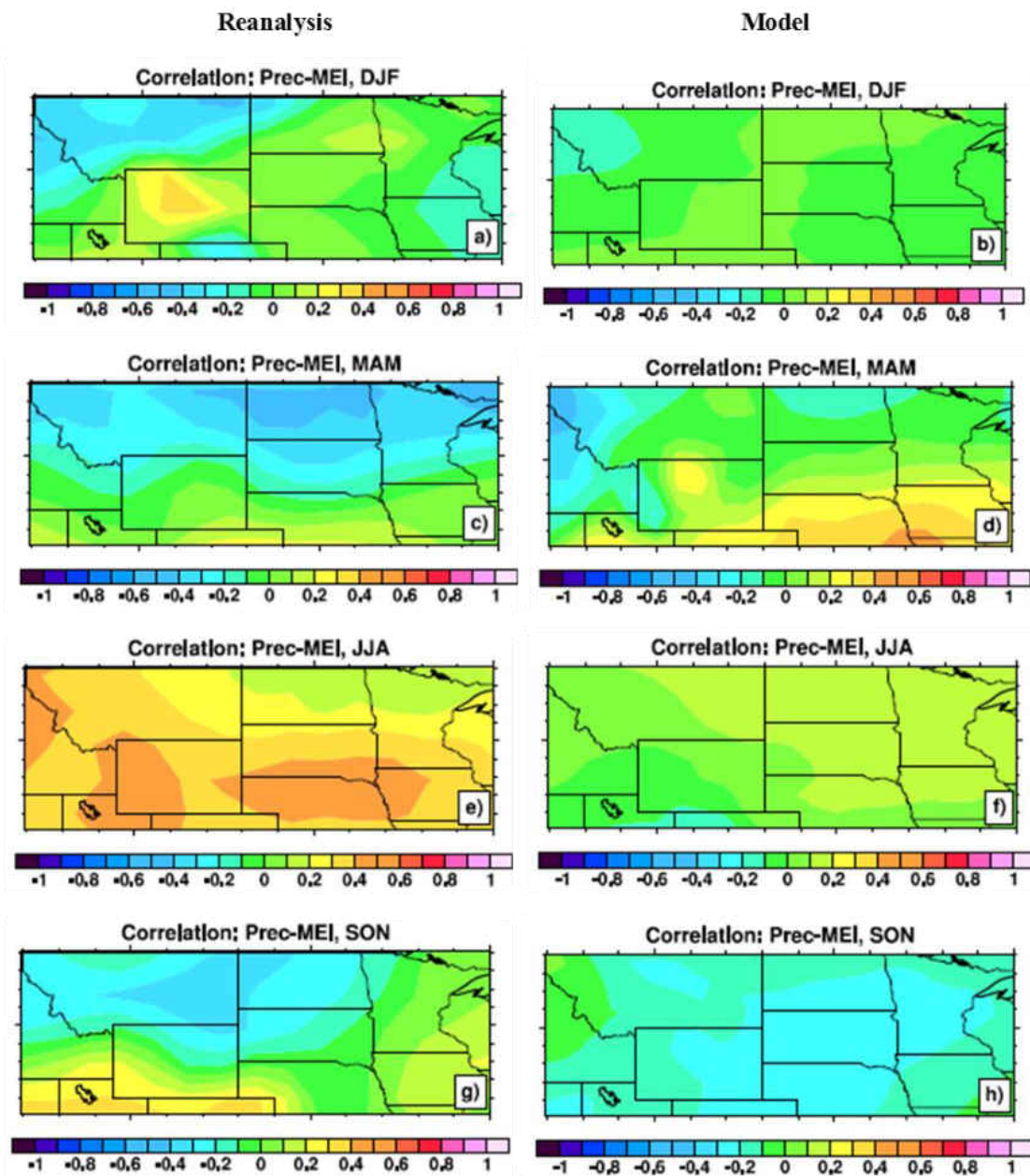


Figure 21. Correlation patterns of four seasonal precipitation anomalies with the MEI for 1965-2005: reanalysis (left) and model (right).

CHAPTER V

CONCLUSIONS

The goal of this study is to investigate changes in temperature and precipitation patterns of the Northern Great Plains (NGP) for the past 41 years (1965-2005) and to study the impact of El-Niño-Southern Oscillation (ENSO) on the detected long-term trends, using reanalysis and the ensemble mean of: the Global Climate Model (GCM; the Community Climate System Model Version 4; the Fourth Generation Canadian Coupled Global Climate Model; and the European Earth System Model) data, along with ground-based observations. The regional temperature and precipitation trends and their linkages to an ENSO index (MEI) are studied from both the conventional linear regression method and an Empirical Orthogonal Function (EOF) analysis. The primary conclusions of this study are summarized as follows:

- (1) An overall warming trend of $\sim 1-2^{\circ}\text{C}$ per 41 years is found across the NGP region using observational and reanalysis data. A seasonal-based EOF analysis, through analyzing reanalysis and ensemble GCM model data, suggests this overall warming trend is contributed mostly by the winter season. No significant warming trends are detected for the other seasons.
- (2) The observational-based analysis shows an increase in annual mean cumulative precipitation of ~ 100 mm/ 41 years over the eastern part of the NGP and a decrease in annual mean cumulative precipitation of ~ -100 mm/ 41 years over the western part of the NGP. A similar pattern is also observed with the use of reanalysis data. An EOF-based analysis suggests that the changes are mostly

contributed from the summer season. Still, this study found rather large discrepancies between model-based and observational/reanalysis data-based precipitation trends. This may indicate that GCM-modeled precipitation fields contain larger uncertainties in comparison with the model-derived temperature fields.

(3) Positive correlations of 0-0.5 are found for the winter and spring seasons between MEI and temperature of the NGP region using the reanalysis data, while negative correlations are found for the other two seasons. Precipitation-wise, significant positive correlations with respect to MEI of 0.25-0.75 are found for the summer season using reanalysis data, while correlations are less significant for other seasons.

(4) The regressions and correlations between MEI and reconstructed (through EOF analysis) temperature and precipitation fields are also estimated. Similar to the linear regression-based analysis, the EOF-based analysis also suggests positive correlations between MEI and temperature/precipitation fields for the winter and spring seasons and strong correlations between MEI and precipitation for the summer season using reanalysis data. This study suggests that ENSO has a strong influence on the changes in NGP's temperature and precipitation patterns.

The regional climate variations and their linkage to ENSO are explored in this study.

Still, ENSO is only one of the many large-scale dynamic patterns that affect the climate of the NGP region. As the next step for this research, the impact of the NAO (North Atlantic Oscillation), AO (Arctic Oscillation), AMO (Atlantic Multidecadal Oscillation),

PDO (Pacific Decadal Oscillation) and MJO (Madden-Julian Oscillation) to the regional climate variations can be evaluated in a similar fashion as mentioned in this study, and thus is a natural extension of this thesis.

REFERENCES

- Bin Yu, Xuebin Zhang, Hai Lin & Jin-Yi Yu (2015) Comparison of Wintertime North American Climate Impacts Associated with Multiple ENSO Indices, *Atmosphere-Ocean*, 3:4, 426-445.
- Bora, G.C., Bali, S. and Mistry, P. (2014) Impact of Climate Variability on Yield of Spring Wheat in North Dakota. *American Journal of Climate Change*, 3, 366-377.
- Bunkers, J. B., J. R. Miller, and A. T. DeGaetano, 1996: An examination of El Niño–La Niña-related precipitation and temperature anomalies across the Northern Plains. *J. Climate*, 9, 147–160.
- Cressman, G.P. 1959. An operational objective analysis system. *Mon. Weather Rev.* 87: 367-374.
- Dommenget D, Latif M. 2002. A cautionary note on the interpretation of EOFs. *Journal of Climate* 15: 216-225.
- Folland, C.K., N.A. Rayner, S.J. Brown, T.M. Smith, S.S. Shen, D.E. Parker, I. Macadam, P.D. Jones, R.N. Jones, N. Nicholls and D.M.H. Sexton, 2001: Global temperature change and its uncertainties since 1861. *Geophys. Res. Lett.*, 28, 2621-2624.

- Goddard, L., S. J. Mason, S. E. Zebiak, C. F. Ropelewski, R. Basher, and M. A. Cane, 2001: Current approaches to seasonal to interannual climate predictions. *Int. J. Climatol.*, 21, 1111-1152.
- Haan, C.T., 2002, *Statistics Methods in Hydrology*, Iowa State Univ Press, Ames, Iowa.
- Hansen, J., et al. (2002), Climate forcings in Goddard Institute for Space Studies SI2000 simulations, *J. Geophys. Res.*, 107D18, 4347.
- Hartmann, D. L. (2015), Pacific sea surface temperature and the winter of 2014, *Geophys. Res. Lett.*, 42.
- Hazeleger, W., and Coauthors, 2010: EC-Earth: A seamless Earth-system prediction approach in action. *Bull. Amer. Meteor. Soc.*, 91, 1357-1363.
- Higgins, R. W., A. Leetmaa, and V. E. Kousky, 2002: Relationships between climate variability and winter temperature extremes in the United States. *J. Climate*, 15, 1555-1572.
- Huang, B., and Coauthors, 2015: Extended Reconstructed Sea Surface Temperature Version 4 (ERSST.v4). Part I: Upgrades and intercomparisons. *J. Climate*, 28, 911–930
- Hurrell, J.W., Kushnir, Y. Ottersen, G., Visbeck, M. (2003): An overview of the North Atlantic Oscillation. *The North Atlantic Oscillation – Climatic Significance and Environmental Impact. Geophysical Monograph 134: 1-35.*
- Hurrell, J. W., and K. E. Trenberth, 1996: Satellite versus surface estimates of air temperature since 1979. *J. Climate*, 9, 2222-2232.

- Kellner, O., and D. Niyogi, 2014: Agroclimatology. Encyclopedia of Natural Resources: Air, Y. Wang, Ed., Taylor & Francis.
- Khairoutdinov, M. and Y. Kogan, 2000: A new cloud physics parameterization in a large-eddy simulation model of marine stratocumulus. *Mon. Wea. Rev.*, 128, 229-243.
- Kistler, R., E. Kalnay, W. Collins, S. Saha, G. White, J. Woollen, M. Chelliah, W. Ebisuzaki, M. Kanamitsu, V. Kousky, H. van den Dool, R. Jenne, and M. Fiorino, 1999: The NCEP-NCAR 50-Year Reanalysis: Monthly Means CD-ROM and Documentation. *Bull. Amer. Meteor. Soc.*, 82, 247-267.
- Krishnamurthy L, Krishnamurthy V (2013) Decadal scale oscillations and trend in the Indian monsoon rainfall. *Clim Dyn* 43:319-331.
- Kushnir, Y., and J. M. Wallace, 1989: Low-frequency variability in the Northern Hemisphere Winter: Geographical distribution, structure and time-scale dependence. *J. Atmos. Sci.*, 46, 3122-3143.
- Lobell DB, Asner GP (2003) Climate and management contributions to recent trends in U.S. agricultural yields. *Science* 299: 1032.
- Lobell DB, Cahill KN, Field CB (2007) Historical effects of temperature and precipitation on California crop yields. *Clim Change* 81: 187-203.
- Lohmann, U. and E. Roeckner, 1996: Design and performance of a new cloud microphysics scheme developed for the ECHAM general circulation model, *Climate Dyn.*, 12, 557-572.
- Merryfield, W. J., W.-S. Lee, G. J. Boer, V. V. Kharin, J. F. Scinocca, G. M. Flato, R. S. Ajayamohan, and J. C. Frye, 2013: The Canadian Seasonal to Interannual

- Prediction System. Part I: Models and initialization. *Mon. Wea. Rev.*, 141, 2910–2945
- Namias, J. 1982. Anatomy of Great Plains protracted heat waves (especially the 1980 U.S. summer drought). *Monthly Weather Review* 110:824-38.
- National Climatic Data Center, Summary of the day, first order, TD-3210, Asheville, N. C., 2000a.
- North, G. R., T. L. Bell, R. F. Cahalan, and F. J. Moeng, 1982: Sampling errors in the estimation of empirical orthogonal functions. *Mon. Wea. Rev.*, 110, 699-706.
- North Dakota Department of Agriculture, (2007), ‘Testimony of Roger Johnson Agriculture Commissioner.’ House Concurrent Resolution 3005.
- Ropelewski, C. F., and M. S. Halpert, 1986: North American precipitation and temperature patterns associated with the El Niño/Southern Oscillation (ENSO). *Mon. Wea. Rev.*, 114, 2352-2362.
- Rotstayn, L.D., 1997: A physically based scheme for the treatment of stratiform clouds and precipitation in large-scale models. I: Description and evaluation of the microphysical processes. *Q. J. R. Meteorol. Soc.*, 123, 1227-1282.
- Sheffield, J., and Coauthors, 2013a: North American climate in CMIP5 experiments. Part I: Evaluation of historical simulations of continental and regional climatology. *J. Climate*, 26, 9209–9245.
- Sheffield, J., and Coauthors, 2013b: North American climate in CMIP5 experiments. Part II: Evaluation of historical simulations of intraseasonal to decadal variability. *J. Climate*, 26, 9247-9290.

- Shields, C. A., Bailey, D. A., Danabasoglu, G., Jochum, M., Kiehl, J. T., Levis, S., and Park, S, 2012: The Low Resolution CCSM4, *J. Climate*, 25, 3993–4014.
- Smith, T. M., R. W. Reynolds, R. E. Livezey, and D. C. Stokes, 1996: Reconstruction of historical sea surface temperatures using empirical orthogonal functions. *J. Climate*, 9, 1403-1420.
- Taguchi, X., and D. L. Hartmann, 2006: Increased occurrence of stratospheric sudden warmings during El Niño as simulated by WACCM. *J. Climate*, 19, 324-332.
- Taylor, K. E., R. J. Stouffer, and G. A. Meehl, 2009: A summary of the CMIP5 experiment design. PCDMI Rep., 33 pp.
- Taylor, K. E., R. J. Stouffer, and G. A. Meehl, 2012: An overview of CMIP5 and the experiment design. *Bull. Amer. Meteor. Soc.*, 93, 485-498.
- Torralba V, Rodríguez-Fonseca B, Mohino E and Losada T (2015) The non-stationary influence of the Atlantic and Pacific Niños on North Eastern South American rainfall. *Front. Earth Sci.* 3:55.
- Vocke, Gary, and Mir Ali. U.S. Wheat Production Practices, Costs, and Yields: Variations Across Regions, EIB-116. U.S. Department of Agriculture, Economic Research Service, August 2013.
- von Salzen, K., N. A. McFarlane, and M. Lazare, 2005: The role of shallow convection in the water and energy cycles of the atmosphere, *Clim. Dyn.*, 25, 671-688.
- Wang, H., and M. F. Ting, 2000: Covariabilities of winter U.S. precipitation and Pacific sea surface temperatures. *J. Climate*, 13, 3711-3719.

- Wang, H., A. Kumar, W. Wang, and B. Jha (2012), U.S. summer precipitation and temperature patterns following the peak phase of El Niño, *J. Clim.*, 25, 7204-7215.
- Wang, S.-Y., M. L'Heureux, and H-H Chia, 2012: ENSO prediction one year in advance using Western North Pacific sea surface temperatures. *Geophysical Research Letters*, 39, L05702.
- Wolter, K., and M. S. Timlin, 1998: Measuring the strength of ENSO events - how does 1997/98 rank? *Weather*, 53, 315-324.
- Yoden, S., M. Taguchi, and Y. Naito (2002), Numerical studies on time variations of the troposphere-stratosphere coupled system, *J. Meteorol. Soc. Jpn.*, 80(4B), 811–30.